

Molecular mechanism of Danxiong Tongmai Granules in treatment of coronary heart disease

Jiahao Ye^{1,*}, Ruiping Yang^{2,*}, Lin Li¹, Senjie Zhong³, Ruixue Jiang², Zhixi Hu¹

¹College of Chinese Medicine, Hunan University of Chinese Medicine, Changsha, Hunan 410208, China

²Basic Medical Sciences College, Hubei University of Chinese Medicine, Wuhan, Hubei 430065, China

³The First Affiliated Hospital of Guangzhou University of Chinese Medicine, Guangzhou University of Chinese Medicine, Guangzhou, Guangdong 510405, China

*Equal contribution

Correspondence to: Zhixi Hu; email: 003405@hnu cm.edu.cn

Keywords: Danxiong Tongmai Granules, coronary heart disease, network pharmacology, molecular docking, molecular dynamics simulation

Received: June 26, 2023

Accepted: February 21, 2024

Published: May 21, 2024

Copyright: © 2024 Ye et al. This is an open access article distributed under the terms of the [Creative Commons Attribution License](https://creativecommons.org/licenses/by/4.0/) (CC BY 4.0), which permits unrestricted use, distribution, and reproduction in any medium, provided the original author and source are credited.

ABSTRACT

Background: Danxiong Tongmai Granules (DXTMG) are widely utilized in treating coronary heart disease (CHD) in China. This study aims to explore the molecular mechanisms underlying the therapeutic effects of DXTMG on CHD by employing a network pharmacology approach, complemented with experimental validation.

Methods: Traditional Chinese Medicine (TCM) compounds and targets were identified via searches in the BATMAN-TCM database, and the GeneCards database was used to obtain the main target genes involved in CHD. We combined disease targets with the drug targets to identify common targets. The “TCM-compound-target” network was plotted using Cytoscape 3.7.2 software and a protein-protein interaction (PPI) network was constructed using the STRING database from which core targets were obtained. Gene ontology (GO) function analysis and Kyoto Encyclopedia of Genes and Genomes (KEGG) pathway enrichment analysis were performed for common drug-disease targets using R Version 4.0.4 (64 bit) software. Molecular docking of core protein-small molecule ligand interaction was modeled using AutoDock software. A molecular dynamics simulation was conducted on the optimal protein-small molecule complex identified through molecular docking, using Amber18 software. The rat model for myocardial ischemia was established through pre-gavage administration of DXTMG, followed by dorsal hypodermic injection of isoprenaline. Myocardial tissues from the rats were analyzed using hematoxylin and eosin (HE) staining and Masson’s trichrome staining. Relevant targets were validated by enzyme-linked immunosorbent assay (ELISA) and immunohistochemistry.

Results: 162 potential targets of DXTMG involved in CHD were identified. These included INS, ALB, IL-6 and TNF according to PPI network studies. GO enrichment analysis identified a total of 3365 GO pathways, including 3049 biological process pathways (BP) concerned with the heart and circulatory system; 109 cellular component (CC) pathways, including cation channels and membrane rafts and 207 molecular function (MF) pathways related to receptor ligands and activators. KEGG analysis revealed a total of 137 pathways ($P < 0.05$), including those related to AGE-RAGE signaling associated with diabetic complications, fluid shear stress and atherosclerosis. The results of molecular docking and molecular dynamics simulations demonstrated the robust binding affinity between the compounds and target proteins. Animal experiment findings indicated that, compared with the model group, the DXTMG group effectively ameliorated inflammation and fibrosis in rat myocardial tissues, reduced LDH, cTn-I, and MDA levels ($P < 0.05$, $P < 0.01$), elevated SOD and GSH-PX levels ($P < 0.05$), and reduced the percentage of positive area for IL-6 and TNF- α ($P < 0.05$).

Conclusion: This study preliminarily suggests that DXTMG can modulate oxidative stress, inflammation response, and cardiomyocyte regulation, thereby mitigating the onset and progression of CHD.

INTRODUCTION

Coronary heart disease (CHD) occurs when atherosclerosis causes luminal stenosis or occlusion, leading to insufficient blood supply to the coronary artery and failure to meet the demands of myocardial metabolism [1]. According to the American Heart Association, 15.5 million adults in the United States suffered from CHD in 2016 [2]. CHD has a serious impact on the patient's quality of life and is characterized by poor prognosis causing high morbidity and mortality rates. Therapeutic approaches commonly taken by Western medicine have many side effects, especially during long-term administration. For example, a 4-month course of statins may contribute to liver damage with raised ALT and AST levels and the development of hepatocyte necrosis, liver fibrosis and increased inflammatory responses [3]. Moreover, there is an increased risk of new-onset diabetes [4]. By contrast, Traditional Chinese Medicine (TCM) often has multi-target and multi-pathway synergistic effects and low incidence of toxic side effects. Thus, TCM has great potential for the treatment of CHD.

Danxiong Tongmai Granules (DXTMG) have gained increasing popularity for treating CHD. Yao et al. [5] treated 171 patients with angina pectoris due to coronary heart disease using DXTMG. The effective rate for exertional angina treatment was 97.28%, while for spontaneous angina, it was 95.83%. Following DXTMG administration, there was a significant reduction in nitroglycerin dosage, and partial discontinuation of the drug was observed. Furthermore, Tang et al. [6] demonstrated that DXTMG effectively lowers systolic and diastolic blood pressure, reduces heart rate, enhances the aorta's elasticity index, and contributes to the protection against cardiovascular and cerebrovascular diseases. Additionally, Shi et al. [7] investigated the effects of DXTMG on hypertensive patients. Platelet activation levels were measured using flow cytometry, revealing a significant reduction in PACI+ % and CD62P+ % levels post-treatment, approaching normal levels. Moreover, improvements in blood lipids and glucose levels were observed. To date, research on DXTMG has primarily focused on clinical observation, with limited progress in elucidating its molecular mechanisms.

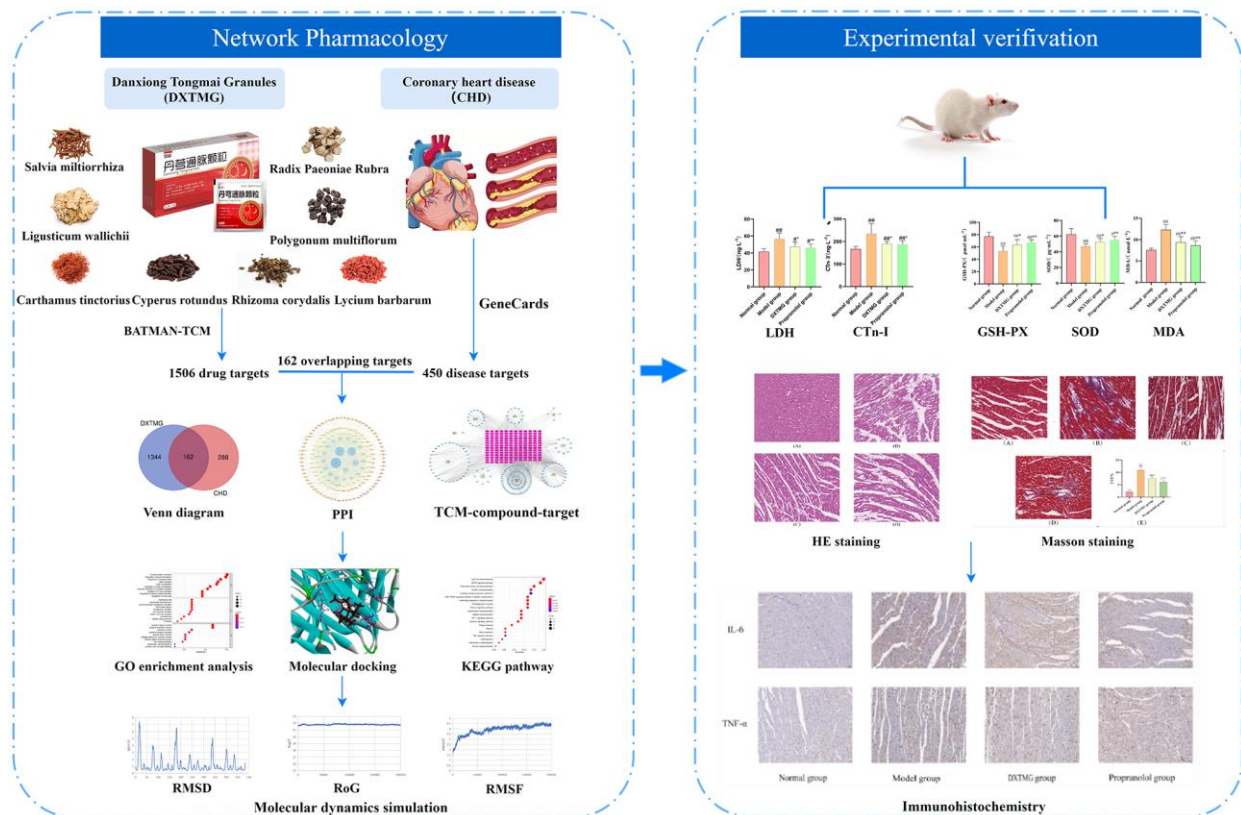


Figure 1. Workflow chart of DXTMG for the potential treatment of coronary heart disease based on network pharmacology.

Network pharmacology is a novel pharmaceutical research method for the systematic analysis of “multi-component-multi-target-multi-pathway” characteristics and has been applied to TCM [8, 9]. Molecular docking is an approach whereby small ligand molecules are modeled within the receptor binding site so that spatial interactions may be explored. Using flexible and semi-flexible docking, receptor-ligand interactive forces may be assessed enabling prediction of binding mode and affinity [10]. Molecular dynamics allows the simulation of various ligand and receptor movements via Newtonian mechanics to assess stability and flexibility. During the present study, core target receptors and ligands were identified through network pharmacology, and interaction sites and binding characteristics were analyzed using molecular docking and molecular dynamics simulations. Finally, the relevant targets were validated through animal experiments to explore the mechanism of DXTMG in treating CHD. The flowchart is shown in Figure 1.

METHODS

Chemical compounds and target genes

The components of DXTMG comprise Radix Paeoniae Rubra, Ligusticum wallichii, Salvia miltiorrhiza, Polygonum multiflorum, Rhizoma corydalis, Cyperus rotundus, Carthamus tinctorius, and Lycium barbarum. Parameters set in the BATMAN-TCM database include a Score cutoff of the system-recommended minimum score of 20 and an adjusted *P*-value threshold value of 0.05 [11].

Targets of CHD

A total of 450 CHD target genes were obtained from the GeneCards database (<https://www.genecards.org/>) using “coronary heart disease” as the keyword and the criterion of Score >30 [12]. Target genes common to both DXTMG and CHD were identified using the Venny diagram online tool (<http://bioinformatics.psb.ugent.be/webtools/Venn/>), and a Venny diagram was generated.

Construction of “TCM-compound-target” network

The effective compounds and drug targets were imported into Cytoscape 3.7.2 software and a “TCM-compound-target” network diagram was plotted [13]. The built-in tool, Network Analyzer, was used to analyze the associations.

Construction of “protein-protein” interaction (PPI) network

Common target proteins were imported into the STRING database (<https://www.string-db.org/>) [14] to

construct a PPI network. The species was set to “Homo sapiens”, and the confidence level was set to >0.4. Unconnected nodes were hidden, and the PPI network diagram was plotted using Cytoscape 3.7.2 software.

Gene ontology (GO) and Kyoto Encyclopedia of Genes and Genomes (KEGG) analysis

GO and KEGG analysis were conducted using R package of clusterProfiler [15]. GO enrichment analysis covered biological process (BP), molecular function (MF) and cellular component (CC). The top 10 GO and the top 20 KEGG pathways were identified ($p < 0.05$).

Molecular docking

The five compounds with the highest scores in the “TCM-Compound-Target” network diagram and the four core proteins with the highest scores in the PPI network underwent molecular docking analysis using AutoDock software [16]. The ligand file was downloaded from the PubChem database (<https://pubchem.ncbi.nlm.nih.gov/>), and energy minimization of the ligand was performed using Chem3D software. Subsequently, the ligand was saved in pdb format, and the charge was calculated using AutoDockTools 1.5.6 software and saved in pdbqt format. The 3D crystal structure of the core target was obtained from the RCSB PDB database (<http://www.rcsb.org/>) and saved in pdb format. Parameters related to the active pocket were determined, and semi-flexible molecular docking was conducted to calculate the “ligand-receptor” binding energy. Finally, the best docking model was generated using Discovery Studio 4.5 software. Binding energies were categorized as follows: >-5 for initial binding, >-7 for stronger binding, and >-9 for very strong binding [17]. The molecular docking results were calculated three times, and the mean value and standard deviation were computed and expressed as “mean value ± standard deviation”.

Molecular dynamics simulation

The Amber18 software package was used to perform molecular dynamics simulation on the protein (target) and small molecule ligand (compound) obtained by molecular docking. ff14SB and general Amber force field (GAFF) parameters were used for proteins and small molecule ligands, respectively, and the AM1-BCC atomic charge was calculated using the ANTECHAMBER module. The protein-ligand complex was loaded into the leap module, and hydrogen atoms and antagonist ions were automatically added to neutralize the charge. The TIP3P explicit water model was selected, and periodic boundary conditions were

set. The workflow of molecular dynamics simulation included energy minimization, heating, equilibration and production dynamics. Heavy atoms of proteins were constrained, and water molecules were subjected to 10,000 steps of energy minimization (including 5000-step steepest descent method and 5000-step conjugate gradient method). The system was slowly heated to 300 K within 50 ps and equilibrated for 50 ps under the NPT ensemble. Molecular dynamics simulation was conducted on the system under the NPT ensemble for 200 ns (25,000 steps in total) with a time step of 2 fs. The trajectory data were saved every 10 ps, followed by analysis using the CPPTRAJ module. The free energy of binding for ligands and proteins was calculated using the MMPBA.py module.

Experimental validation

Animals

Forty male SD rats of SPF grade, aged 6–8 weeks and weighing 200 ± 20 g, were provided by Hunan Slaughter Kingda Laboratory Animal Co. Ltd, under Laboratory Animal Use License No. SCXK (Hunan) 2019-0004. The rats were bred at the Animal Experiment Center of Hunan University of Traditional Chinese Medicine and fed a standard diet. This experiment was reviewed and approved by the Experimental Animal Ethics Committee of Hunan University of Traditional Chinese Medicine, with Ethics Approval No. LL202310250002. The experimental design and procedures adhered to the Hunan Experimental Animal Regulations and the National Institutes of Health Guidelines for the Ethical Use of Animals.

Drugs

Danxiong Tongmai Granules (Sichuan Enwei Pharmaceutical Co., Ltd., 5 g/bag, Lot No. Z20010180); propranolol (Jiangsu Yabang Apsen Pharmaceutical Co., Ltd., Lot No. E230516); isoprenaline (Shanghai Aladdin Biochemical Technology Co., Ltd., Lot No. I129810).

Reagents

Rat Superoxide Dismutase (SOD) ELISA Kit, Rat Lactate Dehydrogenase (LDH) ELISA Kit, Rat Malondialdehyde (MDA) ELISA Kit, Rat Cardiac Troponin I (cTn-I) ELISA Kit, Rat Glutathione Peroxidase (GSH-PX) ELISA Kit (Hunan Alfon Bio Co., Ltd., batch no. Ltd, lot number: AF20230731); TNF- α Primary Antibody Kit (Aifang Bio, lot number: AF06294); IL-6 Primary Antibody Kit (Xavier Bio Co., Ltd, lot number: GB11117); HRP-Polymer Anti-Rat Secondary Antibody Kit (Aifang Bio, lot number: AFIHC002); HRP-Polymer Anti-Rabbit Secondary Antibody Kit (Aifang Bio, Lot No.: AFIHC003);

anhydrous ethanol, xylene, n-butanol, neutral gum (Sinopharm Chemical Reagent Co., Ltd., Lot Nos. 100092683, 10023418, 100052190, and 10004160, respectively); Masson's staining solution kit (Servicebio, Lot No.: G1006); Hematoxylin Differentiation Solution, Hematoxylin Blue Return Solution, Citrate Buffer (Hunan Aifang Biotechnology Co., Ltd, lot numbers: AFIHC019, AFIHC020, AFIHC009); BSA (Servicebio, lot number: G5001).

Instruments

Dehydrator (Wuhan Junjie Electronics Co., Ltd., model: JJ-12J); embedding machine (Wuhan Junjie Electronics Co., Ltd., model: JB-P5); pathology sectioning machine (Shanghai Leica Instruments Co., Ltd., model: RM2016); orthogonal optical microscope (Nikon, Japan, model: Nikon Eclipse E100); enzyme labeling machine (Labsystems Multiskan MS, Model: Model 352).

Grouping, modeling and drug administration

Forty male SD rats aged 6–8 weeks with SPF grade, weighing 200 ± 20 g, were used. After 3 days of acclimatization, the rats were randomly divided into the following groups: normal group, model group, propranolol group (10 mg/kg), and DXTMG group (2.7 g/kg), each consisting of 10 rats. The corresponding dose of the drug (10 mL/kg) was administered by gavage in each treatment group, while the normal and model groups received an equal volume of saline once daily for 7 consecutive days. Two hours after drug administration on the 6th day, isoproterenol (85 mg/kg) was subcutaneously injected into the backs of the rats in the propranolol group, the DXTMG group, and the model group for 2 consecutive days. An equal volume of saline was injected subcutaneously into the normal group [18]. Twenty-four hours after modeling completion, the rats were anesthetized again, blood was collected from the fundus venosus plexus, the rats were euthanized, and their hearts were extracted. The hearts were fixed with 4% paraformaldehyde, excess tissue was excised on ice, leaving only the left ventricle, which was washed with saline and stored in a -80°C freezer for subsequent detection of relevant indexes.

Serum LDH and cTnI level detection

The rats' blood was allowed to stand at room temperature for 2 hours, centrifuged at 4°C and 4000 rpm for 15 minutes, and the supernatant was extracted. Serum LDH and cTnI levels were detected using a microplate assay.

HE staining

Myocardial tissue was fixed with 4% paraformaldehyde, embedded in conventional paraffin, and sectioned into 3 μm thick slices. Subsequently, the

sections were dewaxed to water and stained with hematoxylin for 3~5 minutes. Differentiation was achieved with hydrochloric acid in an aqueous solution followed by blue return using ammonia. The sections were then dehydrated with a gradient of ethanol and stained with eosin staining solution for 5 minutes. Finally, the sections were dehydrated, sealed, and images were captured using a digital section scanner to observe tissue inflammation, degeneration, and necrosis.

Masson staining

Following dewaxing, sections with a thickness of 3 μm were immersed in potassium dichromate at 60°C for 30 minutes. Subsequently, they were stained with ferric hematoxylin for 3 minutes, washed with water, and immersed in Lichun red acidic magenta solution for 5–10 minutes. Afterward, the sections were placed in phosphomolybdic acid aqueous solution for 1–3 minutes and then transferred to aniline blue staining solution for 3–6 minutes. Differentiation was carried out using 1% icosahexaenoic acid, followed by transparent sealing and image acquisition.

Detection of SOD, GSH-Px activity and MDA level in myocardial tissue

An appropriate amount of frozen myocardial tissue was taken, weighed, homogenized, and centrifuged at 4°C and 5000 rpm for 10 minutes. The supernatant was extracted, and the SOD, GSH-Px activity, and MDA level in myocardial tissue were detected according to the instructions of the kit.

Immunohistochemistry method to detect myocardial tissue inflammatory factors IL-6, TNF- α protein

Tissue Inflammatory Factors IL-6 and TNF- α Protein Myocardial tissue paraffin sections were dewaxed to water, and repair solution was added into the autoclave, boiled for 2 minutes, and naturally cooled at room temperature. Subsequently, the sections were removed, and after natural cooling, they were placed in PBS (pH 7.4) in a decolorizing shaker for three washes, each lasting 5 minutes. The sections were then immersed in 3% hydrogen peroxide solution and incubated at room temperature in the dark for 15 minutes, followed by three washes, each for 5 minutes. In the histochemical circle, 3% BSA was added to evenly cover the tissues and incubated at room temperature for 30 minutes. The primary antibodies (IL-6 primary antibody prepared in PBS at a dilution of 1:100, TNF- α primary antibody prepared in PBS at a dilution of 1:200) were incubated overnight at 4°C. After three washes, each for 5 minutes, the sections were slightly dried, and the secondary antibody was added dropwise into the circle. The sections were then incubated for 50 minutes at room temperature, washed with PBST, and color

development was initiated by DAB. The color development was terminated with PBST, and the nuclei were stained with hematoxylin for 2 minutes. After washing, the blue color was restored to the nucleus by reverse deconjugation. The sections were then incubated at room temperature, and the cells were stained with hematoxylin for 2 minutes, washed with water, warmed with warm water, re-blued, reverse dewaxed, hydrated, sealed with clear neutral gum, and photographed. IL-6 and TNF- α positive cells appeared as yellow or brownish-yellow granules in the cytoplasm, while the Normal group did not show such staining. ImageJ software was used for analysis.

Statistical analysis

Statistical analysis was conducted using SPSS 24.0 software, and the data were expressed as $\bar{x} \pm s$. Group comparisons were performed using the *t*-test for two-group comparisons and one-way ANOVA for multiple-group comparisons. $P < 0.05$ indicates that the difference is statistically significant.

Data availability

All data generated or analyzed during this study are available from public databases, published articles and Supplementary Materials.

RESULTS

Screening of active pharmaceutical ingredients and targets

Compounds from DXTMG retrieved from the BATMAN-TCM database included 9 compounds from Radix Paeoniae Rubra, 91 from Ligusticum wallichii, 39 from Salvia miltiorrhiza, 16 from Polygonum multiflorum, 37 from Rhizoma corydalis, 12 from Cyperus rotundus, 22 from Carthamus tinctorius and 1 from Lycium barbarum. Seven replicates were removed leaving 220 compounds in total (Supplementary Table 1). In addition, a total of 11,121 drug targets were retrieved, including 127 targets of Radix Paeoniae Rubra, 2163 of Salvia miltiorrhiza, 4970 of Ligusticum wallichii, 300 of Polygonum multiflorum, 1533 of Rhizoma corydalis, 1074 of Cyperus rotundus, 913 of Carthamus tinctorius, and 41 of Lycium barbarum. Removal of replicates left a total of 1506 targets.

Screening of CHD target genes and construction of “TCM-Disease” intersect targets

A total of 6810 CHD targets were obtained from the GeneCards database. After those with a relevance score >30 had been screened out, a total of 450 targets

remained. A total of 162 targets common to DXTMG and CHD were identified using the Venny online tool (Figure 2).

Determination of targets of DXTMG active components and “TCM-compound-target” network construction

The data were visualized by Cytoscape 3.7.2 software. A “TCM-compound-target” network (Figure 3) was constructed, and its nodes were analyzed. The

compounds with the top 5 Degrees were Tanshinone IIA, Neotanshinone C, Neocryptotanshinone II, Miltonone I and Patchoulenone (Supplementary Table 2). These compounds are likely to be the major chemical components of DXTMG with efficacy in the treatment of CHD.

PPI network analysis

The 162 CHD target proteins of DXTMG were imported into the STRING database and resulting data were

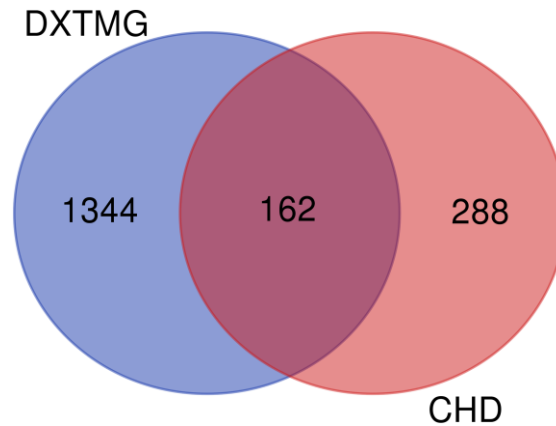


Figure 2. Venny diagram of DXTMG (blue) and CHD targets (red).

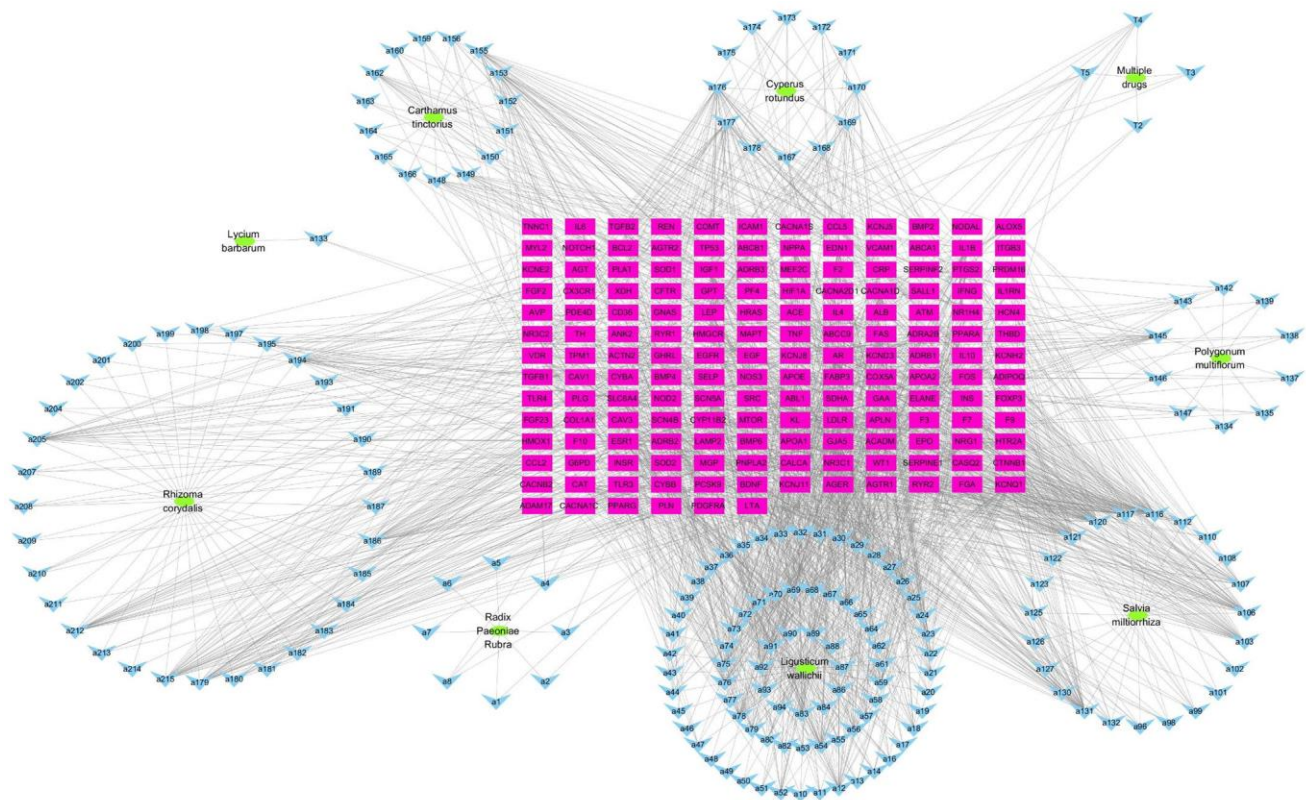


Figure 3. “TCM-compound-target” network diagram. (Green ovals represent TCM; blue inverted triangles represent compound; red rectangles represent targets).

imported into Cytoscape 3.7.2 software. A PPI network diagram was constructed (Figure 4). Core targets with the top 4 Degrees were INS, Alb, IL-6 and TNF.

GO enrichment and KEGG pathway enrichment analysis

The results of GO enrichment analysis showed that there were 3365 GO pathways in total, including 3049 pathways of BP (heart and circulatory system), 109 pathways of CC (cation channels and membrane rafts) and 207 pathways of MF (receptor ligand and activator). The relationships between BP and targets are shown in Figure 5, and the GO analysis results of BP, CC and MF are shown in Figure 6.

A total of 137 KEGG pathways were obtained. DXTMG mainly regulated the Lipid and athero-

sclerosis, MAPK signaling pathway, Fluid shear stress and atherosclerosis, and Diabetic cardiomyopathy. The top 20 KEGG pathways are shown in Figure 7.

Molecular docking

Molecular docking was conducted for core compounds: Tanshinone IIA, Neotanshinone C, Neocryptotanshinone II, Miltionone I, and Patchoulenone, along with core targets: INS, Alb, IL-6, and TNF. The binding energies were <-7 kcal/mol, indicating a strong binding capacity between the compounds and targets. Among them, the binding strength between TNF-Neocryptotanshinone II was the highest, followed by TNF-Patchoulenone and TNF-Tanshinone IIA. The binding site of TNF-Neocryptotanshinone II is a hydrophobic binding site with residues,

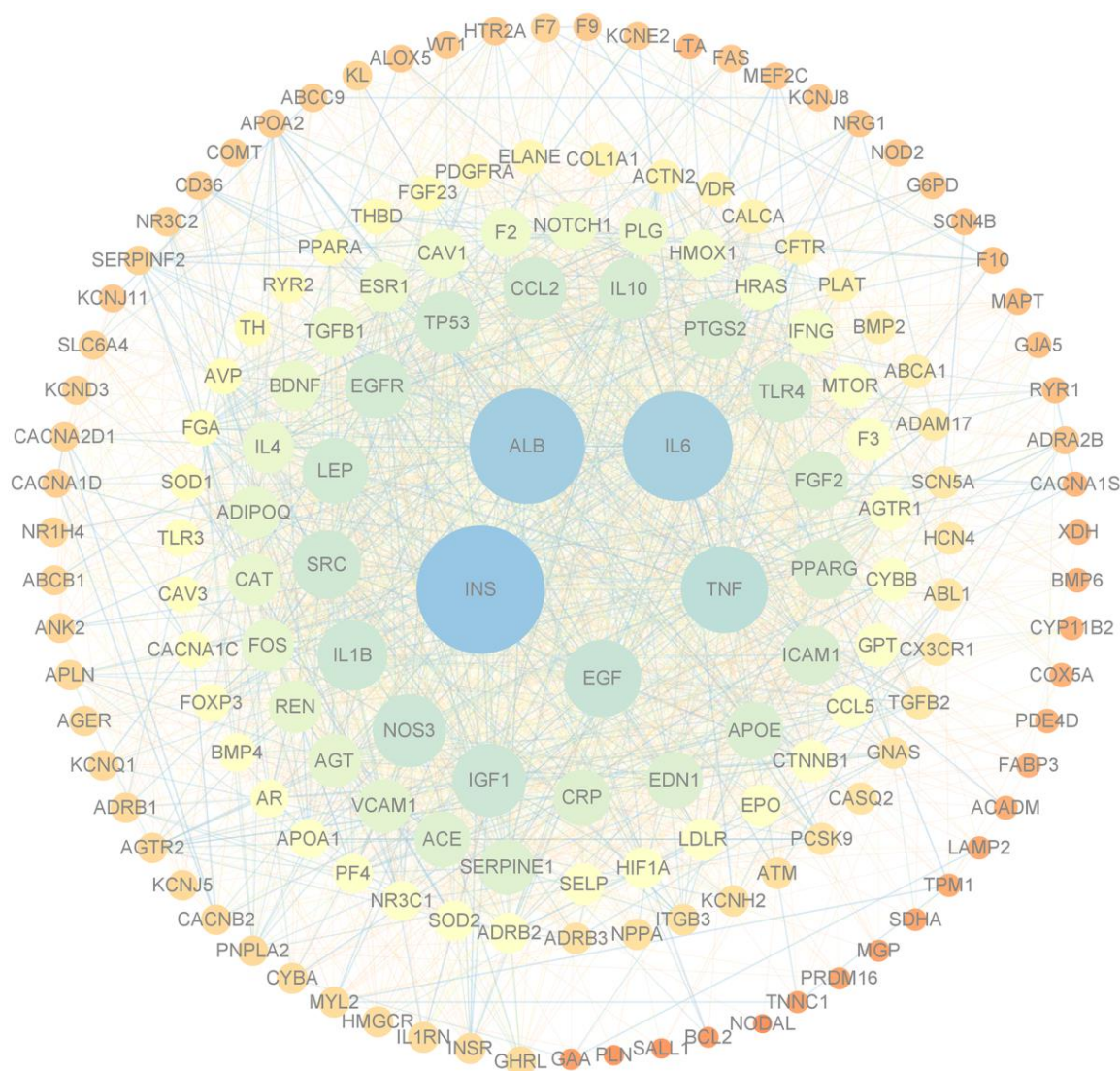


Figure 4. PPI network of targets of DXTMG and CHD. (The sizes and colors of the nodes and lines are illustrated from large to small and blue to red in descending order of degree values).

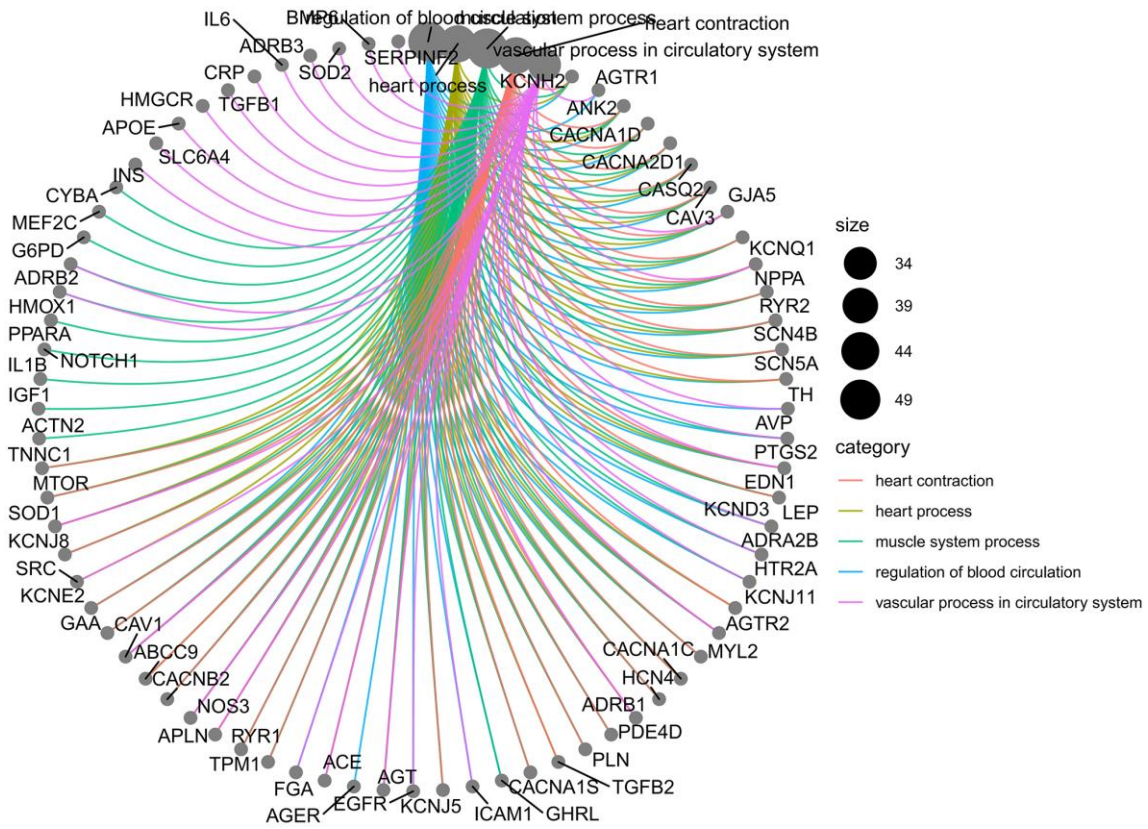


Figure 5. Relationship between BP and targets.

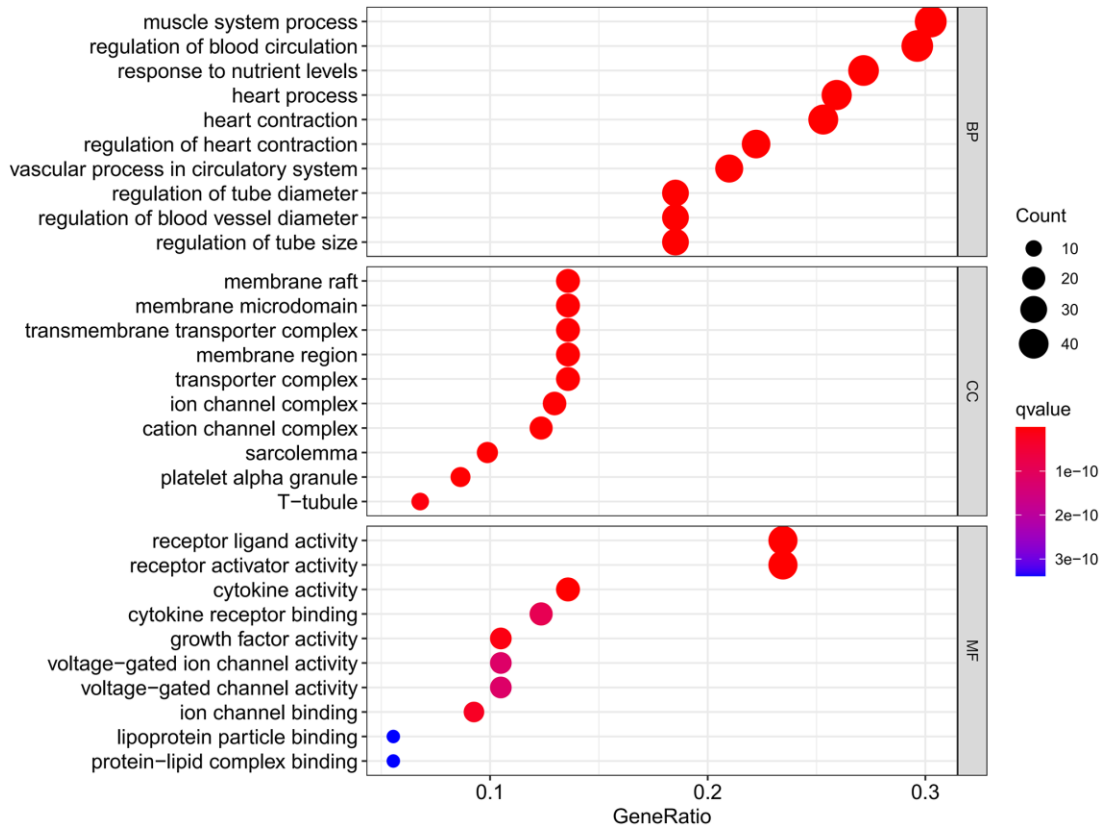


Figure 6. GO analysis results.

forming hydrophobic interactions including Leu481, Phe480, Val482, Phe319, Leu320, Val321, etc. Additionally, the 2D diagram illustrates that the ligand's hydroxyl group can form a hydrogen bond with Leu320, thereby significantly stabilizing its binding. In contrast, the binding site of TNF-Patchoulone is hydrophilic, with hydrophilic residues interacting with ligands such as LYS186, LYS191, and hydrophobic residues like TYR254, PHE298. For TNF-Tanshinone IIA, the binding site presents as amphiphilic, with both hydrophilic and hydrophobic characteristics. Hydrophobic residues encompass Ile378, Val377, while hydrophilic residues include Asn368, Glu454, etc.

The molecular docking results of the compounds and target proteins are detailed in Supplementary Table 3, and the molecular docking diagram is depicted in Figure 8.

Molecular dynamics simulation

Based on binding energy results, molecular dynamics simulation was performed for TNF-Neocryptotanshinone II, TNF-Patchoulone, and TNF-Tanshinone IIA. The root-mean-square deviation (RMSD), radius of gyration (Rog), root-mean-square fluctuation (RMSF) curve and binding free energy were calculated.

The RMSD curve represented variations in protein conformation. The results show that the RMSD fluctuations are relatively gentle, and the RMSD fluctuations of the TNF-Neocryptotanshinone II protein are relatively gentle, especially after 80 ns, such that the RMSD is stable around 4~4.5 Å. The fluctuations in RMSD of TNF-Patchoulone and TNF-Tanshinone IIA proteins are relatively gentle, especially after 100 ns, such that the RMSD is stable around 3~3.5 Å. This result shows that the binding of the small molecule to the receptor protein does not lead to a sustained and significant change in its conformation. The RMSD results are shown in Figure 9.

The Rog curve displayed the compactness of the overall protein structure. The radius of gyration of TNF-Neocryptotanshinone II and TNF-Patchoulone slightly decreased, indicating that the binding of small molecules to the receptor may make the receptor protein structure more compact. However, the radius of gyration of TNF-Tanshinone IIA did not change significantly, indicating that the binding of the small molecule to the receptor had no effect on the protein conformation. The ROG results are shown in Figure 10.

The RMSF curve displays variations in the conformation of amino acid residues. Several smaller

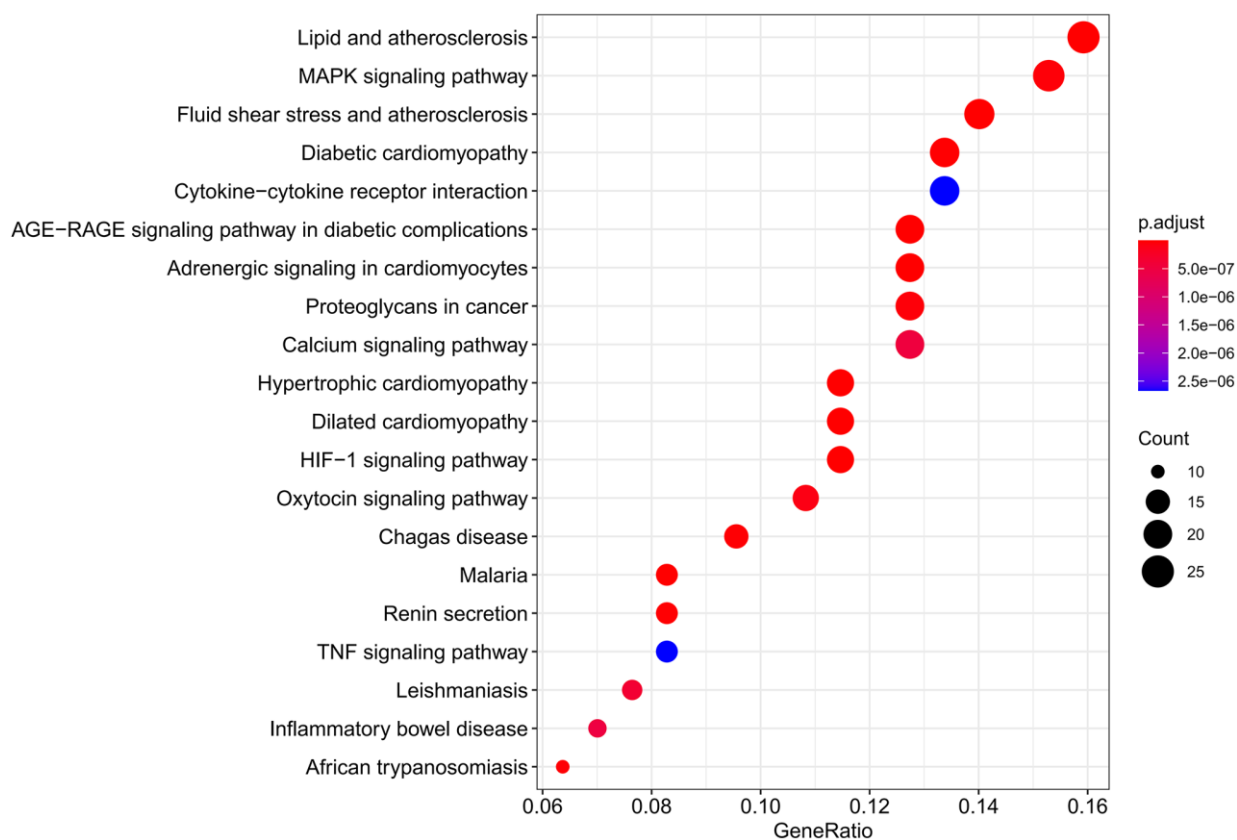


Figure 7. Results of KEGG pathway enrichment analysis.

regions of the protein core domain of TNF-Neocryptotanshinone II, TNF-Patchoulone, and TNF-Tanshinone IIA have greater flexibility than other regions, and these regions include 0–25, 70–80, 170–180 and 390–410; most of these regions are loop-based, so they have high flexibility. The RMSF results are shown in Figure 11.

Protein conformational changes: After a 200-ns molecular dynamics simulation process, TNF and Neocryptotanshinone II form a tight bond. The kinetics did not alter the binding site or the binding stability of the small molecule, demonstrating enhanced binding to the receptor protein. The binding sites of TNF and Patchoulone exhibited slight alterations, yet the small

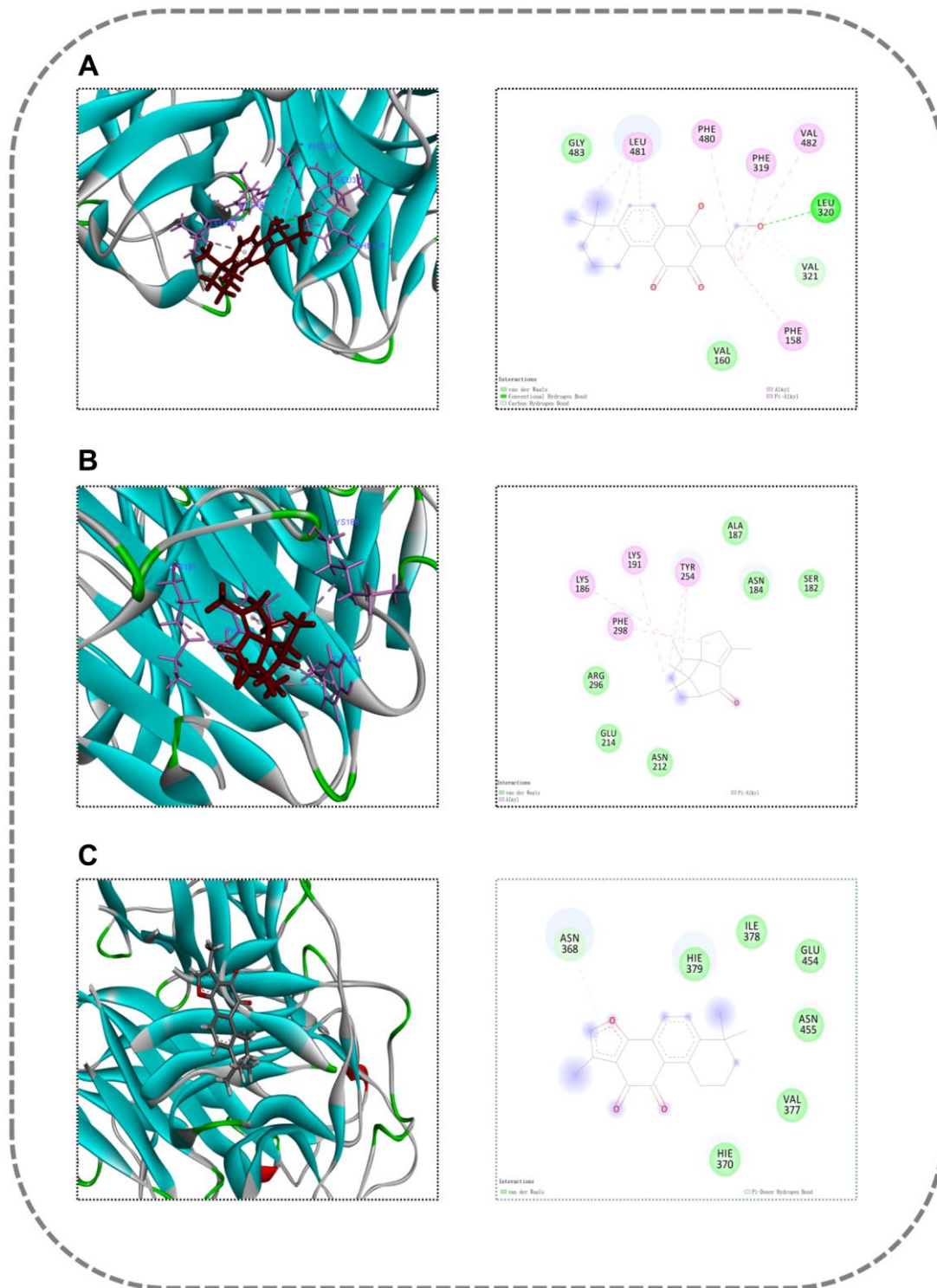


Figure 8. Molecular docking diagram. (A) TNF-Neocryptotanshinone II; (B) TNF-Patchoulone; (C) TNF-Tanshinone IIA.

molecule consistently maintained tight binding to the receptor protein without detachment, indicating improved binding. Conversely, the binding sites of TNF and Tanshinone IIA underwent significant changes, and the small molecules exhibited a tendency to detach, indicating poor binding to the receptor protein, consistent with the binding free energy data. The results of the protein conformational changes are shown in Figure 12.

HE staining results

As shown in Figure 13, the cardiac tissue of the control group exhibited uniformly colored cardiac myofibers, distinct cell demarcations, clear transverse striations of cardiomyocytes, and well-defined bright and dark areas,

with no abnormalities observed in the interstitium. Furthermore, no obvious necrosis or inflammatory cell infiltration was detected. In contrast, the model group displayed multifocal necrosis of cardiomyocytes, cell fragmentation, nucleus fragmentation and lysis, along with increased inflammatory cell infiltration in the interstitium. In the DXTMG group, there was a small amount of inflammatory cell infiltration in the interstitium.

Effects of DXTMG on serum LDH and cTnI levels in rats with acute myocardial ischemia

As shown in Figure 14, serum LDH and cTnI levels were elevated in the model group compared to the

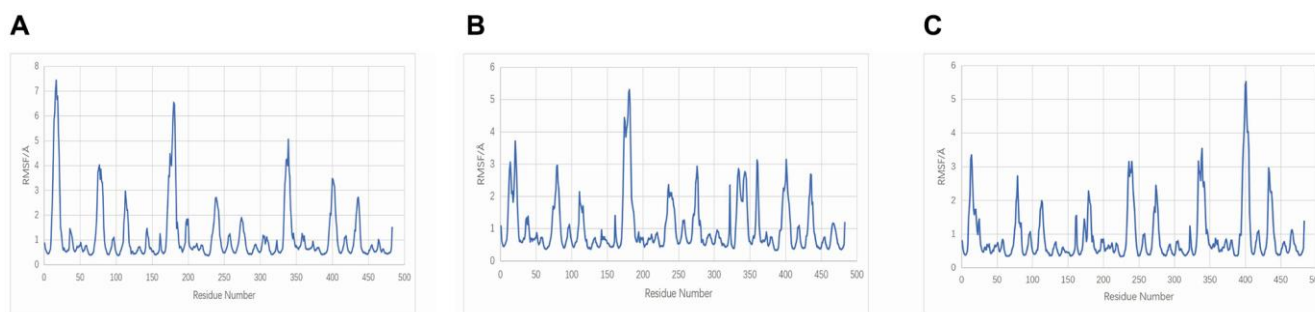


Figure 9. RMSD plot during molecular dynamics simulations. (A) TNF-Neocryptotanshinone II; (B) TNF-Patchoulonone; (C) TNF-Tanshinone IIA.

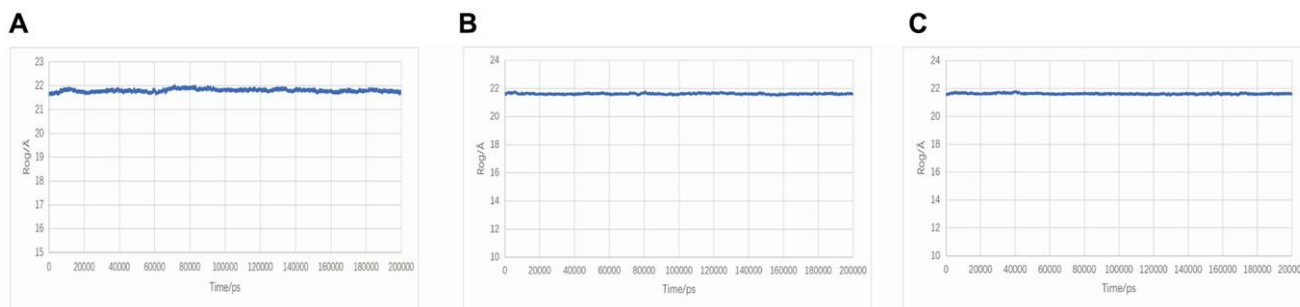


Figure 10. Rog plot during molecular dynamics simulations. (A) TNF-Neocryptotanshinone II; (B) TNF-Patchoulonone; (C) TNF-Tanshinone IIA.

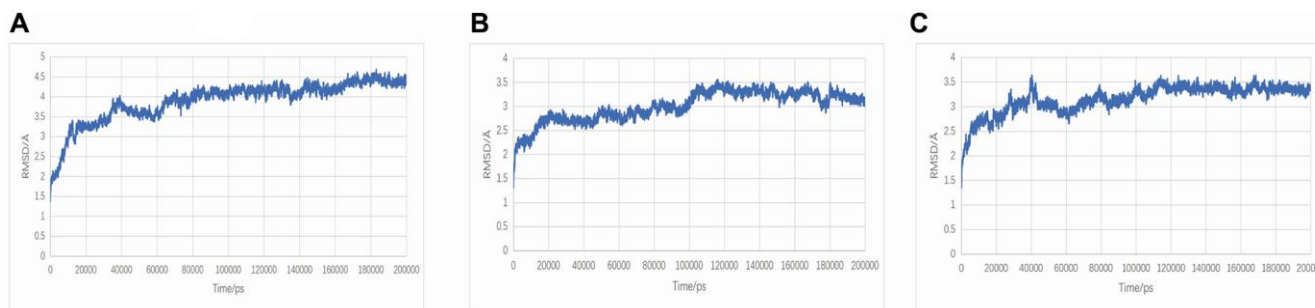


Figure 11. RMSF plot during molecular dynamics simulations. (A) TNF-Neocryptotanshinone II; (B) TNF-Patchoulonone; (C) TNF-Tanshinone IIA.

normal group ($P < 0.01$). Conversely, serum LDH and cTnI levels were reduced in the DXTMG group compared to the model group ($P < 0.05$, $P < 0.01$).

MASSON staining results

As shown in Figure 15, myocardial fibers in the Normal group were neatly arranged, with clearer transverse lines and no obvious collagen deposition. In contrast, the model group exhibited disordered myofiber arrangement, fibrotic interstitium, and severe collagen deposition. However, in the DXTMG group, the

myofiber arrangement was partially disordered, with a small amount of collagen deposition observed. The area of collagen deposition in each group was quantified, revealing a reduction in the DXTMG group compared to the model group ($P < 0.05$).

Effects of DXTMG on SOD, GSH-Px activity and MDA levels in myocardial tissues of rats with acute myocardial ischemia

As shown in Figure 16, compared to the Normal group, myocardial tissue SOD and GSH-Px activities in rats of

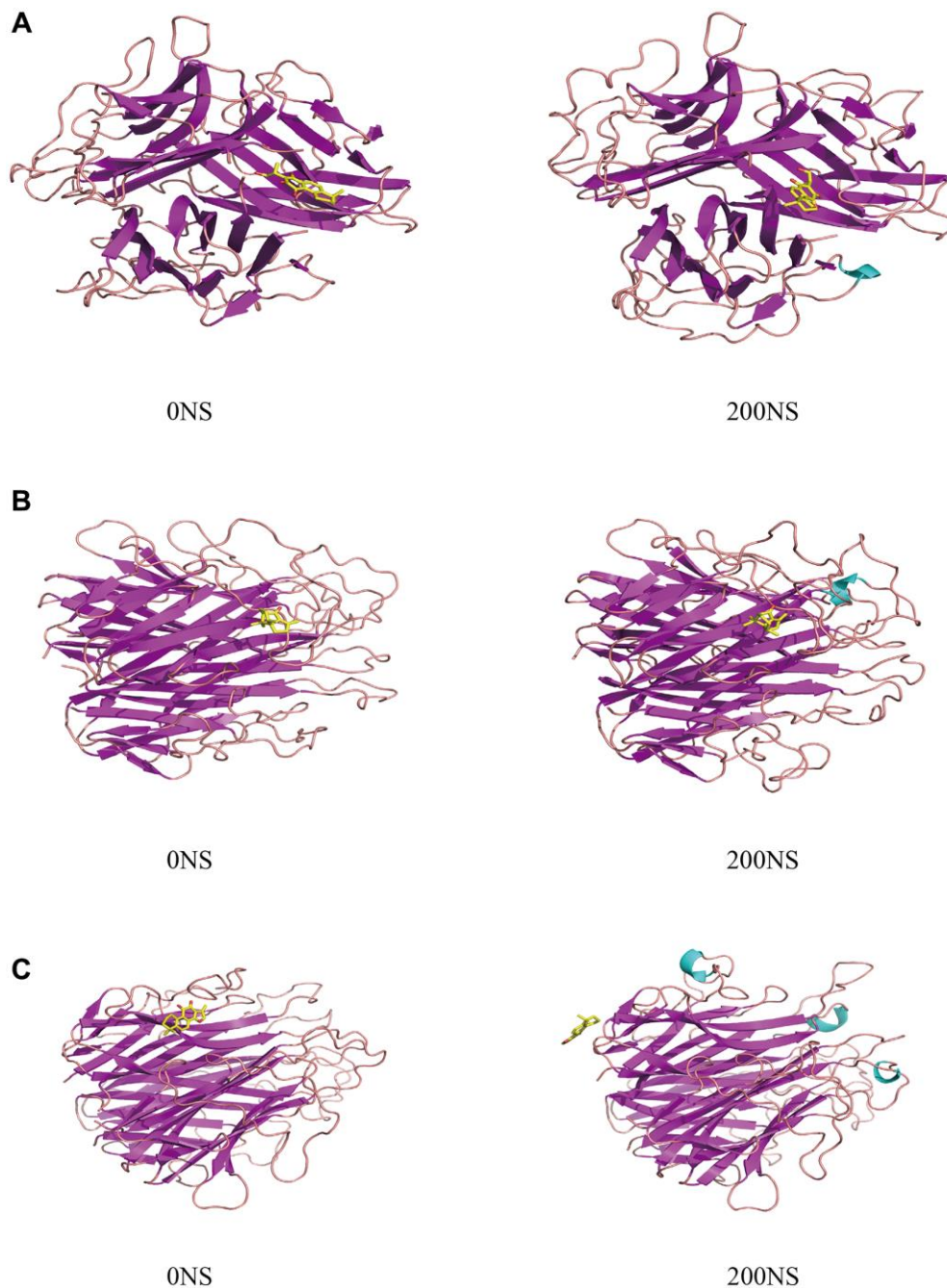


Figure 12. The protein conformational changes results. (A) TNF-Neocryptotanshinone II; (B) TNF-Patchoulone; (C) TNF-Tanshinone IIA.

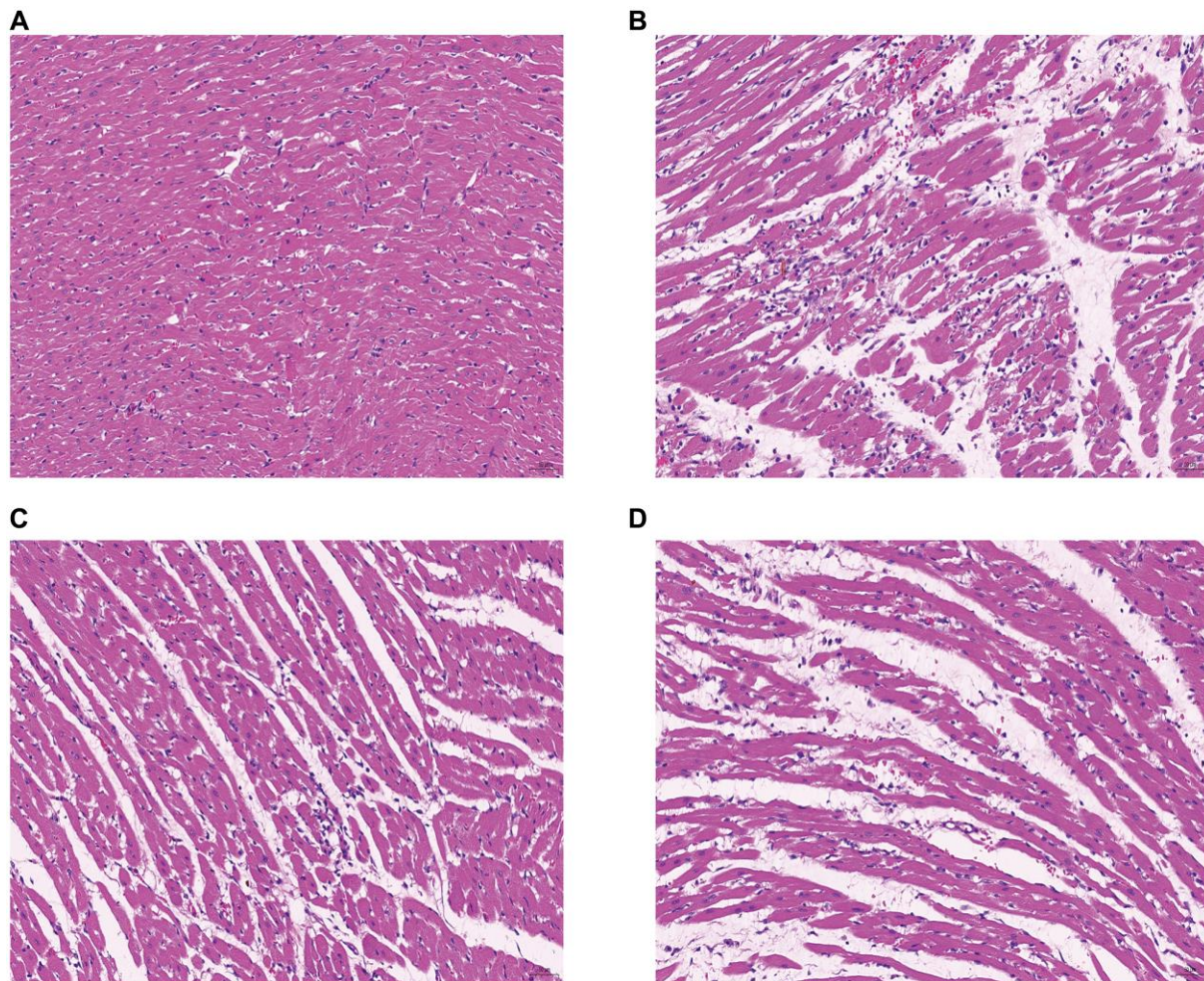


Figure 13. Morphology of rat cardiomyocytes in each group (HE staining, ×20). (A) Normal group (B) Model group (C) DXTMG group (D) Propranolol group.

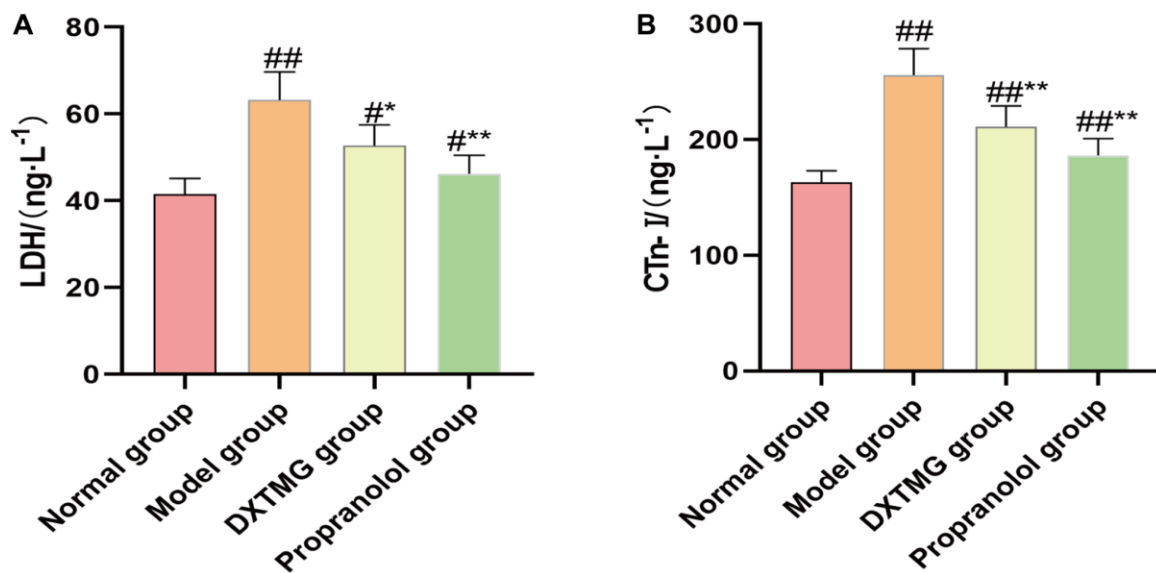


Figure 14. Plasma LDH and CTn-I levels in the normal group, the model group, the DXTMG group and the propranolol group. (A) lactate dehydrogenase (LDH); (B) Cardiac troponin I (CTn-I). Data are presented as the mean ± S.D. (n = 8). ##P < 0.01 vs. Normal group; #P < 0.05 vs. Normal group; **P < 0.01 vs. Model group; *P < 0.05 vs. Model group.

the Model group were decreased ($P < 0.01$), while MDA levels were increased ($P < 0.01$). In comparison to the Model group rats, myocardial tissue SOD and GSH-Px activities in the DXTMG group were increased ($P < 0.05$), and MDA levels were decreased ($P < 0.01$).

Immunohistochemistry results

As shown in Figures 17 and 18, a small number of brownish-yellow positive particles appeared in the cytoplasm of myocardial tissue cells in the Normal

group rats. In comparison to the Normal group, the relative expression of IL-6 and TNF- α positive cells in the myocardial tissue of Model group rats increased ($P < 0.01$). Conversely, compared to the Model group, the relative expression of IL-6 and TNF- α positive cells in the myocardial tissue of DXTMG group rats decreased ($P < 0.05$).

DISCUSSION

The current study presents evidence that Tanshinone IIA, Neotanshinone C, Neocryptotanshinone II,

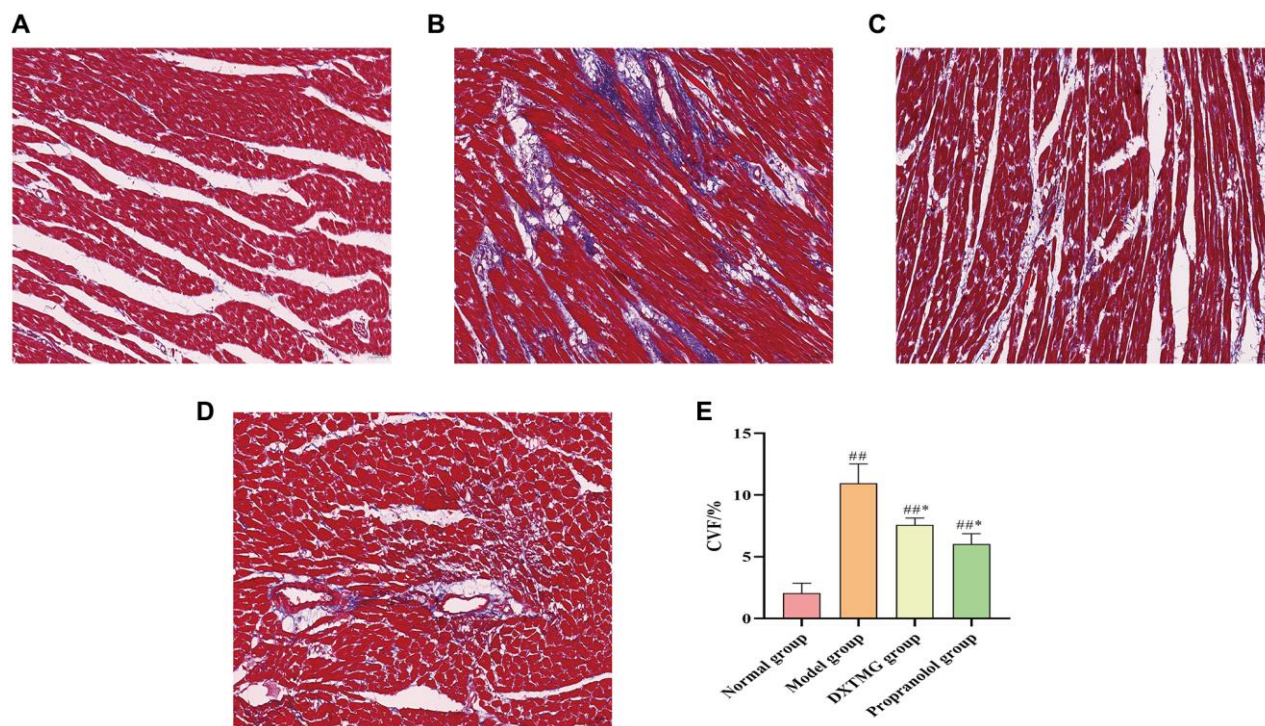


Figure 15. Morphology of rat cardiomyocytes in each group (Masson staining, $\times 20$). (A) Blank group; (B) Model group; (C) DXTMG group; (D) Propranolol group; (E) Comparison of CVF in rats of various groups.

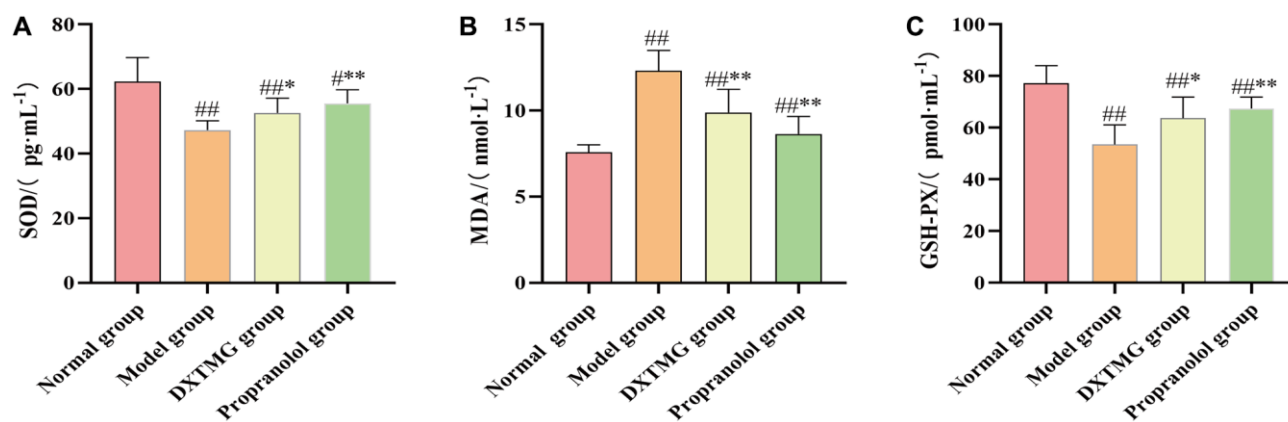


Figure 16. Myocardium SOD, MDA, and GSH-PX levels in the normal group, model group, DXTMG group, and propranolol group. (A) Rat Superoxide Dismutase (SOD); (B) Malondialdehyde (MDA); (C) Glutathione Peroxidase (GSH-PX). Data are presented as the mean \pm S.D. ($n = 8$). $^{###}P < 0.01$ vs. Normal group; $^{**}P < 0.01$ vs. Model group; $^{*}P < 0.05$ vs. Model group.

Miltionone I, and Patchoulone are the major compounds of DXTMG with potential pharmacological activity. Previous work at the cellular level has established that Tanshinone IIA greatly relieves myocardial inflammatory infiltration and oxidative damage caused by myocardial ischemia-reperfusion injury in rats and reduces leakage of lactate dehydrogenase and production of MDA, thereby protecting against myocardial ischemia-reperfusion injury [19]. Tanshinone IIA has an estrogen-like effect resulting in protein kinase B (Akt) activation and suppression of cardiomyocyte apoptosis on activation by insulin-like growth factor II (IGF-II). This suggests a

role for Tanshinone IIA as a potential selective estrogen receptor modulator in the prevention of myocardial apoptosis and treatment of cardiovascular diseases [20]. Moreover, Li et al. [21] demonstrated a role for Tanshinone IIA in suppressing mitogen-activated protein kinase (MAPK) and down-regulating c-fos expression, thus reducing intimal hyperplasia and vascular smooth muscle cell proliferation in rats with carotid artery balloon injury. Neocryptotanshinone suppresses lipopolysaccharide-induced inflammatory factors, including TNF- α and IL-6, in rats. Neocryptotanshinone also reduces lipopolysaccharide-induced production of nitric oxide [22].

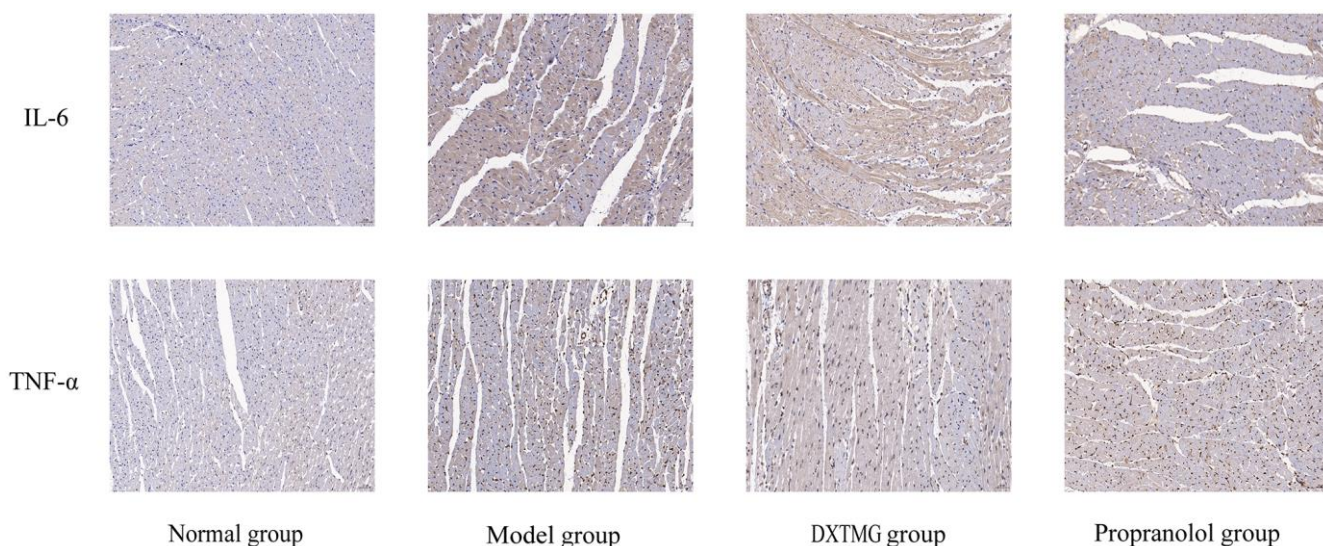


Figure 17. Immunohistochemistry of cellular IL-6 and TNF- α expression in rat cardiomyocytes from 4 groups ($\times 20$).

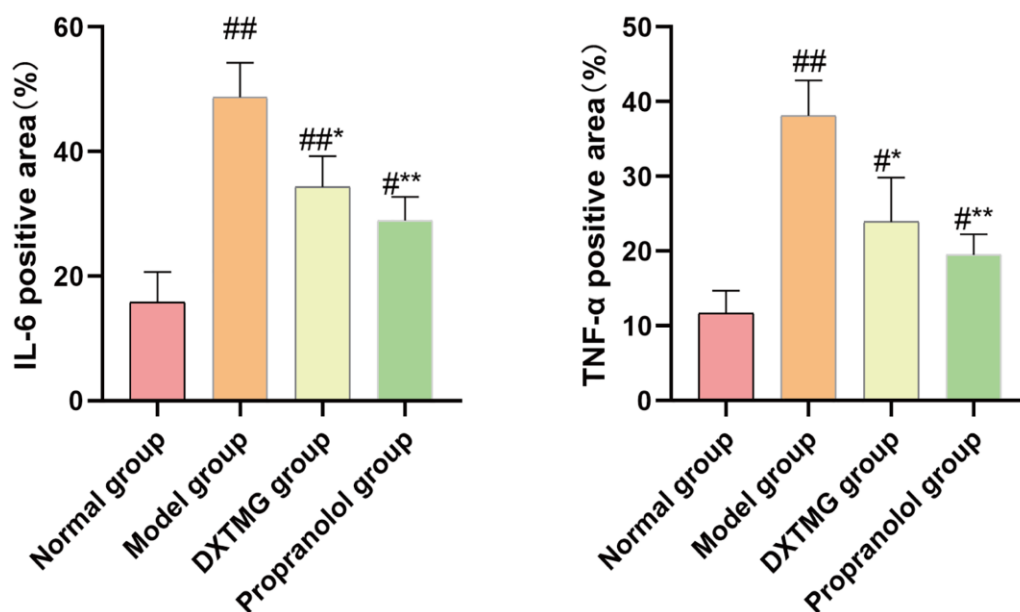


Figure 18. Comparison of the percentage of positive area of IL-6 and TNF- α in myocardial tissue of rats from 4 groups ($\bar{x} \pm s$, $n = 3$).

The pharmacological and computer-based investigations of Maione et al. [23] demonstrated a concentration-dependent activity of Neocryptotanshinone in inhibiting platelet aggregation and antagonizing G protein-coupled P2Y₁₂ platelet ADP receptor.

The PPI analysis in this study identified INS, ALB, IL-6, and TNF as major targets of DXTMG in CHD treatment. Previous studies have established that insulin resistance (IR) serves as a predisposing factor for cardiovascular diseases, including CHD [24]. IR leads to elevated levels of inflammatory cytokines, increased expression of adhesion molecules, imbalanced vascular regulation, and vascular endothelial injury, ultimately culminating in atherosclerosis [25]. INS plays a crucial role in enhancing glucose uptake and utilization, thereby safeguarding the ischemic-hypoxic myocardium. Elevated blood glucose levels pose a risk factor for cardiovascular diseases, and the hypoglycemic effect of INS is pivotal in blood glucose regulation [26]. High levels of INS augment angiotensin II through the renin-angiotensin system and promote the production of reactive oxygen species, thereby facilitating inflammatory and oxidative stress responses [27]. Normal levels of albumin inhibit platelet activation, aggregation, and apoptosis of vascular endothelial cells, thus reducing the risk of CHD [28]. The accumulation of inflammatory cells around damaged vascular tissues may promote plaque formation via the secretion of inflammatory mediators, making inflammatory markers significant risk factors for CHD [29, 30]. Scheller et al. [31] demonstrated a positive correlation between IL-6 levels and the incidence of severe coronary artery lesions. IL-6 promotes macrophage activation and formation of foam cells, stimulates the expression of macrophage low-density lipoprotein receptors, and triggers matrix metalloproteinases to destabilize atheromatous plaques, leading to plaque rupture [32]. Vascular endothelial injury is known to stimulate inflammatory receptors and the release of inflammatory factors, such as TNF- α and IL-6, followed by thrombosis and plaque rupture [33]. The suppression of smooth muscle cell proliferation, which correlates with down-regulated expression of TNF- α and IL-6, may enhance the stability of atherosclerotic plaques [34]. Additionally, IL-6 and TNF- α , as the main pro-inflammatory markers in myocardial injury, induce the recruitment of more neutrophils, monocytes, and lymphocytes from peripheral blood to the injured myocardium, initiating an inflammatory cascade and stimulating a more intense inflammatory response, leading to cardiac hypertrophy, hyperfibrosis, and apoptosis [35].

In this experiment, a rat myocardial ischemia model was established by pretreating with DXTMG via gavage

followed by injection of 85 mg·kg⁻¹ ISO for two consecutive days starting on the 6th day. The protective effect and mechanism of DXTMG on myocardial ischemia were investigated by comparing the results of HE staining, MASSON staining, immunohistochemistry, and ELISA. Currently, dorsal injection of ISO in rats is one of the commonly used models of myocardial ischemic injury. ISO leads to rapid generation and aggregation of a large number of free radicals through its own oxidation, thus inducing myocardial ischemia and hypoxia. This method can simulate the alterations seen in acute myocardial ischemia [36].

cTnI is a regulatory protein specific to myocardial tissue and plays a pivotal role in myocardial contraction [37]. During myocardial ischemia, increased cell membrane permeability allows cTnI and LDH, among other substances, to enter the bloodstream through the cell membrane. These are sensitive and specific serum markers of myocardial cell injury [38].

The results of this experiment showed that serum LDH and cTnI levels were abnormally elevated in the model group rats, indicating obvious myocardial injury. However, DXTMG significantly reduced the release of LDH and cTnI in cardiomyocytes. Additionally, HE staining of rat myocardium in the model group revealed multifocal necrosis of cardiomyocytes, cell fragmentation, cytoplasmic fragmentation and lysis, and increased inflammatory cell infiltration in the interstitium. MASSON staining showed disorganized arrangement of myofibrils, fibrotic changes in the interstitium, and severe collagen deposition. Immunohistochemistry results demonstrated elevated the percentage of IL-6 and TNF- α positive areas; however, DXTMG reduced the percentage of IL-6 and TNF- α positive areas, and attenuated the release of LDH and cTnI in rat myocytes. DXTMG could reduce the expression of IL-6 and TNF- α in rat myocardium and attenuate the inflammatory reaction and fibrotic changes in myocardial tissue, suggesting that anti-inflammation and anti-myocardial fibrosis may be another important target of DXTMG in attenuating myocardial ischemic injury. SOD reflects the body's ability to scavenge free radicals, while MDA reflects the degree of cellular damage caused by free radicals [39]. GSH is the main component of the cellular antioxidant defense system, playing a crucial role in maintaining normal cellular metabolism and regulating the body's immune response [40]. These indicators collectively constitute the body's defense system against oxidative damage caused by free radicals, which is essential for maintaining oxidative/antioxidant homeostasis in the body. The present experiment demonstrated that DXTMG significantly

increased SOD and GSH levels, reduced MDA levels, reestablished the free radical balance, and scavenged oxygen radicals through antioxidant enzymes. This restoration of cardiac function alleviated oxidative damage to cardiomyocytes. In conclusion, the protective effect of DXTMG on isoprenaline-induced acute myocardial ischemia in rats may be related to its scavenging of free radicals, enhancement of antioxidant enzymes, inhibition of inflammatory factor expression, and reduction of inflammatory response.

The current study used KEGG pathway enrichment analysis to demonstrate that fluid shear stress and atherosclerosis, the hypoxia-inducible factor-1 (HIF-1) signaling pathway, adrenergic signaling in cardiomyocytes and the AGE-RAGE signaling pathway in diabetic complications were implicated in the action of DXTMG in CHD treatment. Atherosclerosis is involved in the pathological development of CHD when plaque formation-induced changes in shear stress affect the normal function and phenotype of vascular wall endothelial cells [41]. It has been established that low shear stress up-regulates expression of intercellular adhesion molecule-1 on the endothelial cell surface, promoting activation of endothelial cells [42]. A further consequence is phosphorylation of platelet endothelial cell adhesion molecule-1, activating the MAPK pathway and worsening inflammation to promote CHD. HIF-1, a hypoxia-induced DNA-binding protein, induces increased expression of HIF-1 α during myocardial ischemia and hypoxia, thereby protecting the myocardium [43]. Moreover, HIF-1 induces endothelial cell dysfunction, proliferation, angiogenesis and inflammation, thus playing a role in the pathogenesis of atherosclerosis via various pathways [44]. Via its action on the α 1 receptor in vascular smooth muscle, epinephrine promotes vasoconstriction and increases aortic diastolic pressure, thereby raising coronary perfusion pressure [45]. Adrenergic signaling in cardiomyocytes enhances myocardial contractility, resulting in vascular dilation of both heart and liver and vascular contraction of both skin and mucosa, thereby exerting a therapeutic effect on CHD. Activated AGE/RAGE signaling, which enhances inflammation, oxidative stress and vascular smooth muscle cell apoptosis, thus promoting the development of atherosclerosis, plays a significant role in CHD through the above mechanisms [46].

We present results of molecular docking experiments, which revealed stable binding between components of DXTMG and receptor proteins with the binding energy of the TNF-Neocryptotanshinone II interaction being the highest, followed by TNF-Patchoulone and

TNF-Tanshinone IIA. Molecular dynamics simulations showed that the binding of TNF-Neocryptotanshinone II, TNF-Patchoulone and TNF-Tanshinone IIA was relatively stable.

CONCLUSION

The current study constructed a “TCM-compound-target” network and PPI network to investigate the role of DXTMG in the treatment of CHD using the approach of network pharmacology. Findings were validated by molecular docking and molecular dynamics simulation. Our findings reveal DXTMG can influence oxidative stress, inflammation response and cardiomyocytes regulation, thereby reducing the occurrence and development of CHD, and exposing avenues for further investigation through animal and clinical experiments.

Abbreviations

TCM: Traditional Chinese medicines; DXTMG: Danxiong Tongmai Granules; CHD: Coronary Heart disease; GO: Gene Ontology; KEGG: Kyoto Encyclopedia of Genes and Genomes; PPI: Protein-protein interaction; INS: Insulin; AIB: Albumin; IL6: Interleukin 6; TNF: Tumor necrosis factor; BP: Biological processes; CC: Cellular component; MF: Molecular function; BATMAN-TCM: Bioinformatics Analysis Tool of Molecular mechanism of Traditional Chinese Medicine; GAFF: General Amber Force Field; RMSF: Root mean square fluctuation; RMSD: Root mean square deviation; IGF-II: Insulin-like growth factor II; Akt: Protein kinase; BMAPK: Mitogen-activated protein kinase; IR: Insulin resistance; HIF-1: Hypoxia-inducible factor-1; PDB: Protein Data Bank; SOD: Superoxide Dismutase; LDH: Lactate Dehydrogenase; MDA: Malondialdehyde; cTn-I: Cardiac Troponin I; GSH-PX: Glutathione Peroxidase.

AUTHOR CONTRIBUTIONS

The design of the study was performed by ZXH. JHY collected the data. RPY prepared the figures. The manuscript was written by JHY and RPY. LL, SJZ and RXJ reviewed and edited the manuscript. JHY and RPY contributed equally to this work. All authors have read and approved the final manuscript.

ACKNOWLEDGMENTS

The authors would like to express their gratitude to EditSprings (<https://www.editsprings.com/>) for the expert linguistic services provided. A preprint has previously been published (Ref. No. 784340) [47].

CONFLICTS OF INTEREST

The authors declare no conflicts of interest related to this study.

ETHICAL STATEMENT

This experiment has been reviewed by the Experimental Animal Ethics Committee of Hunan University of Traditional Chinese Medicine, Experimental Ethics Approval No. LL202310250002. The experimental design and implementation were based on the Hunan Experimental Animal Regulations and the National Institutes of Health Guidelines for the Ethical Use of Animals.

FUNDING

This work was supported by grants from the National Natural Science Foundation of China (Grant No. 82274412).

REFERENCES

1. Wirtz PH, von Känel R. Psychological Stress, Inflammation, and Coronary Heart Disease. *Curr Cardiol Rep.* 2017; 19:111.
<https://doi.org/10.1007/s11886-017-0919-x>
PMID:[28932967](https://pubmed.ncbi.nlm.nih.gov/28932967/)
2. Sanchis-Gomar F, Perez-Quilis C, Leischik R, Lucia A. Epidemiology of coronary heart disease and acute coronary syndrome. *Ann Transl Med.* 2016; 4:256.
<https://doi.org/10.21037/atm.2016.06.33>
PMID:[27500157](https://pubmed.ncbi.nlm.nih.gov/27500157/)
3. Schulze J, Glass X. Statin hepatotoxicity and the dilemma of causality in rare hepatic adverse drug reactions. *J Hepatol.* 2012; 57:702–3.
<https://doi.org/10.1016/j.jhep.2012.03.010>
PMID:[22510260](https://pubmed.ncbi.nlm.nih.gov/22510260/)
4. Carter AA, Gomes T, Camacho X, Juurlink DN, Shah BR, Mamdani MM. Risk of incident diabetes among patients treated with statins: population based study. *BMJ.* 2013; 346:f2610.
<https://doi.org/10.1136/bmj.f2610>
PMID:[23704171](https://pubmed.ncbi.nlm.nih.gov/23704171/)
5. Yao P, Zhao CX, Lv QC. Clinical study on Danxiong Tongmai Granulation in Treating Patients with Angina Pectori Caused by Coronary Heart Disease. *China Foreign Medical Treatment.* 2011; 30:22–4.
6. Tang P, Qin W, Zhang TJ. Clinical study about effect of the Dan Xiong Tong Mai granule on cerebrovascular disease and related factors. *Sichuan Medical Journal.* 2009; 30:487–9.
7. Shi GY, Shi XG, Gong YC, Jin HF, Yu JR, Chen F, Zeng Z, Guo YZ. Determination of the level of platelet activation in hypertensive patients treated with Danxiong Tongmai Keli. *Academic Journal of Shanghai Second Medical University.* 2004; 822–5.
8. Hopkins AL. Network pharmacology: the next paradigm in drug discovery. *Nat Chem Biol.* 2008; 4:682–90.
<https://doi.org/10.1038/nchembio.118>
PMID:[18936753](https://pubmed.ncbi.nlm.nih.gov/18936753/)
9. Huang SJ, Mu F, Li F, Wang WJ, Zhang W, Lei L, Ma Y, Wang JW. Systematic Elucidation of the Potential Mechanism of Erzhi Pill against Drug-Induced Liver Injury via Network Pharmacology Approach. *Evidence-Based Complementary and Alternative Medicine.* 2020; 2020.
10. Del Zoppo GJ, Saver JL, Jauch EC, Adams HP Jr, and American Heart Association Stroke Council. Expansion of the time window for treatment of acute ischemic stroke with intravenous tissue plasminogen activator: a science advisory from the American Heart Association/American Stroke Association. *Stroke.* 2009; 40:2945–8.
<https://doi.org/10.1161/STROKEAHA.109.192535>
PMID:[19478221](https://pubmed.ncbi.nlm.nih.gov/19478221/)
11. Liu Z, Guo F, Wang Y, Li C, Zhang X, Li H, Diao L, Gu J, Wang W, Li D, He F. BATMAN-TCM: a Bioinformatics Analysis Tool for Molecular mechANism of Traditional Chinese Medicine. *Sci Rep.* 2016; 6:21146.
<https://doi.org/10.1038/srep21146>
PMID:[26879404](https://pubmed.ncbi.nlm.nih.gov/26879404/)
12. Safran M, Dalah I, Alexander J, Rosen N, Iny Stein T, Shmoish M, Nativ N, Bahir I, Doniger T, Krug H, Sirota-Madi A, Olender T, Golan Y, et al. GeneCards Version 3: the human gene integrator. *Database (Oxford).* 2010; 2010:baq020.
<https://doi.org/10.1093/database/baq020>
PMID:[20689021](https://pubmed.ncbi.nlm.nih.gov/20689021/)
13. Otasek D, Morris JH, Bouças J, Pico AR, Demchak B. Cytoscape Automation: empowering workflow-based network analysis. *Genome Biol.* 2019; 20:185.
<https://doi.org/10.1186/s13059-019-1758-4>
PMID:[31477170](https://pubmed.ncbi.nlm.nih.gov/31477170/)
14. Szklarczyk D, Franceschini A, Wyder S, Forslund K, Heller D, Huerta-Cepas J, Simonovic M, Roth A, Santos A, Tsafou KP, Kuhn M, Bork P, Jensen LJ, von Mering C. STRING v10: protein-protein interaction networks, integrated over the tree of life. *Nucleic Acids Res.* 2015; 43:D447–52.
<https://doi.org/10.1093/nar/gku1003>
PMID:[25352553](https://pubmed.ncbi.nlm.nih.gov/25352553/)

15. Yu G, Wang LG, Han Y, He QY. clusterProfiler: an R package for comparing biological themes among gene clusters. *OMICS*. 2012; 16:284–7.
<https://doi.org/10.1089/omi.2011.0118>
PMID:22455463
16. Trott O, Olson AJ. AutoDock Vina: improving the speed and accuracy of docking with a new scoring function, efficient optimization, and multithreading. *J Comput Chem*. 2010; 31:455–61.
<https://doi.org/10.1002/jcc.21334>
PMID:19499576
17. Gaillard T. Evaluation of AutoDock and AutoDock Vina on the CASF-2013 Benchmark. *J Chem Inf Model*. 2018; 58:1697–706.
<https://doi.org/10.1021/acs.jcim.8b00312>
PMID:29989806
18. Zhang T, Dang M, Zhang W, Lin X. Gold nanoparticles synthesized from *Euphorbia fischeriana* root by green route method alleviates the isoprenaline hydrochloride induced myocardial infarction in rats. *J Photochem Photobiol B*. 2020; 202:111705.
<https://doi.org/10.1016/j.jphotobiol.2019.111705>
PMID:31812087
19. Shen WL, Yu F, Xu L, Chen C, Cao Y, Liu S, Han N, Wang C, Qi R. Protective effects of tanshinone IIA derivative on myocardial ischemia/reperfusion injury in rats. *Journal of Chinese Pharmaceutical Sciences*. 2018; 27:1–13.
20. Weng YS, Kuo WW, Lin YM, Kuo CH, Tzang BS, Tsai FJ, Tsai CH, Lin JA, Hsieh DJ, Huang CY. Danshen mediates through estrogen receptors to activate Akt and inhibit apoptosis effect of Leu27IGF-II-induced IGF-II receptor signaling activation in cardiomyoblasts. *Food Chem Toxicol*. 2013; 56:28–39.
<https://doi.org/10.1016/j.fct.2013.01.008>
PMID:23419388
21. Li X, Du JR, Yu Y, Bai B, Zheng XY. Tanshinone IIA inhibits smooth muscle proliferation and intimal hyperplasia in the rat carotid balloon-injured model through inhibition of MAPK signaling pathway. *J Ethnopharmacol*. 2010; 129:273–9.
<https://doi.org/10.1016/j.jep.2010.03.021>
PMID:20363310
22. Wu C, Zhao W, Zhang X, Chen X. Neocryptotanshinone inhibits lipopolysaccharide-induced inflammation in RAW264.7 macrophages by suppression of NF- κ B and iNOS signaling pathways. *Acta Pharm Sin B*. 2015; 5:323–9.
<https://doi.org/10.1016/j.apsb.2015.01.010>
PMID:26579462
23. Maione F, Cantone V, Chini MG, De Feo V, Mascolo N, Bifulco G. Molecular mechanism of tanshinone IIA and cryptotanshinone in platelet anti-aggregating effects: an integrated study of pharmacology and computational analysis. *Fitoterapia*. 2015; 100:174–8.
<https://doi.org/10.1016/j.fitote.2014.11.024>
PMID:25497578
24. Metwally AH, Elgamel MA. The relation between hepatitis C virus and coronary heart disease. *Med Hypotheses*. 2014; 82:505.
<https://doi.org/10.1016/j.mehy.2014.01.030>
PMID:24559690
25. Thakore AH, Guo CY, Larson MG, Corey D, Wang TJ, Vasan RS, D'Agostino RB Sr, Lipinska I, Keaney JF Jr, Benjamin EJ, O'Donnell CJ. Association of multiple inflammatory markers with carotid intimal medial thickness and stenosis (from the Framingham Heart Study). *Am J Cardiol*. 2007; 99:1598–602.
<https://doi.org/10.1016/j.amicard.2007.01.036>
PMID:17531588
26. Li TT, Xu J, Qin XF. Insulin protects heart against ischemia/reperfusion injury through stimulation of glucose metabolism. *Chinese Heart Journal*. 2017; 29:534–8.
27. Hu SJ, Peng YZ, Yu Y. Clinical trial of Danshen dripping pill in the treatment of diabetic coronary heart disease. *The Chinese Journal of Clinical Pharmacology*. 2017; 33:486–9.
28. Barbano B, Gigante A, Amoroso A, Cianci R. Thrombosis in nephrotic syndrome. *Semin Thromb Hemost*. 2013; 39:469–76.
<https://doi.org/10.1055/s-0033-1343887>
PMID:23625754
29. Ren ZH, Tong YH, Xu W, Ma J, Chen Y. Tanshinone II A attenuates inflammatory responses of rats with myocardial infarction by reducing MCP-1 expression. *Phytomedicine*. 2010; 17:212–8.
<https://doi.org/10.1016/j.phymed.2009.08.010>
PMID:19800776
30. Li H, Sun K, Zhao R, Hu J, Hao Z, Wang F, Lu Y, Liu F, Zhang Y. Inflammatory biomarkers of coronary heart disease. *Front Biosci (Schol Ed)*. 2018; 10:185–96.
<https://doi.org/10.2741/s508>
PMID:28930526
31. Scheller J, Chalaris A, Schmidt-Arras D, Rose-John S. The pro- and anti-inflammatory properties of the cytokine interleukin-6. *Biochim Biophys Acta*. 2011; 1813:878–88.
<https://doi.org/10.1016/j.bbamcr.2011.01.034>
PMID:21296109
32. Feng HP, Jia XW, Xie JM. Effect of Rosuvastatin on IL-6, GMP-140, BNP and Cardiac Function in Elderly

- Patients with Acute Coronary Syndrome. Chinese Journal of Gerontology. 2015; 35:5769–70.
33. Mudau M, Genis A, Lochner A, Strijdom H. Endothelial dysfunction: the early predictor of atherosclerosis. *Cardiovasc J Afr.* 2012; 23:222–31.
<https://doi.org/10.5830/CVJA-2011-068>
PMID:[22614668](https://pubmed.ncbi.nlm.nih.gov/22614668/)
 34. Wang XP, Zhang W, Liu XQ, Wang WK, Yan F, Dong WQ, Zhang Y, Zhang MX. Arginase I enhances atherosclerotic plaque stabilization by inhibiting inflammation and promoting smooth muscle cell proliferation. *Eur Heart J.* 2014; 35:911–9.
<https://doi.org/10.1093/eurheartj/ehz329>
PMID:[23999450](https://pubmed.ncbi.nlm.nih.gov/23999450/)
 35. Jaén RI, Val-Blasco A, Prieto P, Gil-Fernández M, Smani T, López-Sendón JL, Delgado C, Boscá L, Fernández-Velasco M. Innate Immune Receptors, Key Actors in Cardiovascular Diseases. *JACC Basic Transl Sci.* 2020; 5:735–49.
<https://doi.org/10.1016/j.jacbts.2020.03.015>
PMID:[32760860](https://pubmed.ncbi.nlm.nih.gov/32760860/)
 36. Yates JC, Beamish RE, Dhalla NS. Ventricular dysfunction and necrosis produced by adrenochrome metabolite of epinephrine: relation to pathogenesis of catecholamine cardiomyopathy. *Am Heart J.* 1981; 102:210–21.
[https://doi.org/10.1016/s0002-8703\(81\)80012-9](https://doi.org/10.1016/s0002-8703(81)80012-9)
PMID:[7258095](https://pubmed.ncbi.nlm.nih.gov/7258095/)
 37. Lu Q, Pan B, Bai H, Zhao W, Liu L, Li G, Liu R, Lv T, Huang X, Li X, Tian J. Intranuclear cardiac troponin I plays a functional role in regulating *Atp2a2* expression in cardiomyocytes. *Genes Dis.* 2021; 9:1689–700.
<https://doi.org/10.1016/j.gendis.2021.04.007>
PMID:[36157491](https://pubmed.ncbi.nlm.nih.gov/36157491/)
 38. Chaulin A. Cardiac Troponins: Contemporary Biological Data and New Methods of Determination. *Vasc Health Risk Manag.* 2021; 17:299–316.
<https://doi.org/10.2147/VHRM.S300002>
PMID:[34113117](https://pubmed.ncbi.nlm.nih.gov/34113117/)
 39. Smriti K, Pai KM, Ravindranath V, Pentapati KC. Role of salivary malondialdehyde in assessment of oxidative stress among diabetics. *J Oral Biol Craniofac Res.* 2016; 6:41–4.
<https://doi.org/10.1016/j.jobcr.2015.12.004>
PMID:[26937368](https://pubmed.ncbi.nlm.nih.gov/26937368/)
 40. Khatua TN, Padiya R, Karnewar S, Kuncha M, Agawane SB, Kotamraju S, Banerjee SK. Garlic provides protection to mice heart against isoproterenol-induced oxidative damage: role of nitric oxide. *Nitric Oxide.* 2012; 27:9–17.
<https://doi.org/10.1016/j.niox.2012.03.004>
PMID:[22484451](https://pubmed.ncbi.nlm.nih.gov/22484451/)
 41. Chatzizisis YS, Coskun AU, Jonas M, Edelman ER, Feldman CL, Stone PH. Role of endothelial shear stress in the natural history of coronary atherosclerosis and vascular remodeling: molecular, cellular, and vascular behavior. *J Am Coll Cardiol.* 2007; 49:2379–93.
<https://doi.org/10.1016/j.jacc.2007.02.059>
PMID:[17599600](https://pubmed.ncbi.nlm.nih.gov/17599600/)
 42. Meza D, Musmacker B, Steadman E, Stransky T, Rubenstein DA, Yin W. Endothelial Cell Biomechanical Responses are Dependent on Both Fluid Shear Stress and Tensile Strain. *Cell Mol Bioeng.* 2019; 12:311–25.
<https://doi.org/10.1007/s12195-019-00585-0>
PMID:[31719917](https://pubmed.ncbi.nlm.nih.gov/31719917/)
 43. Weidemann A, Johnson RS. Biology of HIF-1alpha. *Cell Death Differ.* 2008; 15:621–7.
<https://doi.org/10.1038/cdd.2008.12>
PMID:[18259201](https://pubmed.ncbi.nlm.nih.gov/18259201/)
 44. Jain T, Nikolopoulou EA, Xu Q, Qu A. Hypoxia inducible factor as a therapeutic target for atherosclerosis. *Pharmacol Ther.* 2018; 183:22–33.
<https://doi.org/10.1016/j.pharmthera.2017.09.003>
PMID:[28942242](https://pubmed.ncbi.nlm.nih.gov/28942242/)
 45. Gough CJR, Nolan JP. The role of adrenaline in cardiopulmonary resuscitation. *Crit Care.* 2018; 22:139.
<https://doi.org/10.1186/s13054-018-2058-1>
PMID:[29843791](https://pubmed.ncbi.nlm.nih.gov/29843791/)
 46. Fishman SL, Sonmez H, Basman C, Singh V, Poretsky L. The role of advanced glycation end-products in the development of coronary artery disease in patients with and without diabetes mellitus: a review. *Mol Med.* 2018; 24:59.
<https://doi.org/10.1186/s10020-018-0060-3>
PMID:[30470170](https://pubmed.ncbi.nlm.nih.gov/30470170/)
 47. Ye J, Yang R, Hu Z, Li L, Zhong S, Jiang R. Molecular Mechanism of Danxiang Tongmai Granules in Treatment of Coronary Heart Disease, 19 August 2021. PREPRINT (Version 1) available at Research Square. 2021.

SUPPLEMENTARY MATERIALS

Supplementary Tables

Supplementary Table 1. Active ingredients of DXTMG.

Drug	Active ingredients	No.	Drug	Active ingredients	No.
Radix Paeoniae Rubra	(-)-Catechin	a1	Salvia miltiorrhiza	Isotanshinone II	a111
Radix Paeoniae Rubra	(+)-Catechin	a2	Salvia miltiorrhiza	Isotenulin	a112
Radix Paeoniae Rubra	Albiflorin	a3	Salvia miltiorrhiza	Lithospermate B	a113
Radix Paeoniae Rubra	Beta-Sitosterol	a4	Salvia miltiorrhiza	Lithospermic Acid	a114
Radix Paeoniae Rubra	Catechin	a5	Salvia miltiorrhiza	Magnesium Lithospermate B	a115
Radix Paeoniae Rubra	Epigallocatechin	a6	Salvia miltiorrhiza	Miltionone I	a116
Radix Paeoniae Rubra	Gallocatechin	a7	Salvia miltiorrhiza	Miltirone	a117
Radix Paeoniae Rubra	Lactiflorin	a8	Salvia miltiorrhiza	Monomethyl Lithospermate	a118
Radix Paeoniae Rubra	Paeonol	a9	Salvia miltiorrhiza	Neocryptotanshinone	a119
Ligusticum wallichii	(Z,Z')-Diligustilide	a10	Salvia miltiorrhiza	Neocryptotanshinone II	a120
Ligusticum wallichii	ta-Hydroxybutyryl)-10-Deacetylba	a11	Salvia miltiorrhiza	Neotanshinone C	a121
Ligusticum wallichii	13-Methyl Pentadecanoic Acid	a12	Salvia miltiorrhiza	Rosmarinine	a122
Ligusticum wallichii	1-Methoxy-2-Methylanthraquinone	a13	Salvia miltiorrhiza	Salonitenolide	a123
Ligusticum wallichii	1-Phenyl-1-Pentanone	a14	Salvia miltiorrhiza	Salvianolicacid B	a124
Ligusticum wallichii	-2,6-Dimethyl-8-(3-Methyl-2-Buten	a15	Salvia miltiorrhiza	Salvinone	a125
Ligusticum wallichii	24-Ethylidene Lophenol	a16	Salvia miltiorrhiza	Salviol	a126
Ligusticum wallichii	3(S)-3-Butyl-4,5-Dihydrophthalide	a17	Salvia miltiorrhiza	Samaderin A	a127
Ligusticum wallichii	3-Carene	a18	Salvia miltiorrhiza	Tanshinone II A	a128
Ligusticum wallichii	droxy-4,5,6,7-Tetrahydro-6,7-Dihy	a19	Salvia miltiorrhiza	Tanshinone II B	a129
Ligusticum wallichii	5,6-Dihydroergosterol	a20	Salvia miltiorrhiza	Tanshinone VI	a130
Ligusticum wallichii	Alpha-Humulene	a21	Salvia miltiorrhiza	Tanshiquinone B	a131
Ligusticum wallichii	Alpha-Phellandrene	a22	Salvia miltiorrhiza	Ursolicacid	a132
Ligusticum wallichii	Alpha-Pinene	a23	lycium barbarum	Betaine	a133
Ligusticum wallichii	Alpha-Terpinene	a24	Polygonum multiflorum	Chrysarobin	a134
Ligusticum wallichii	Alpha-Terpineol	a25	Polygonum multiflorum	Chrysazin	a135
Ligusticum wallichii	Alpha-Terpinolene	a26	Polygonum multiflorum	Citreorsein	a136
Ligusticum wallichii	Beta-Elemene	a27	Polygonum multiflorum	Emodin	a137
Ligusticum wallichii	Beta-Eudesmol	a28	Polygonum multiflorum	Emodin Anthrone	a138
Ligusticum wallichii	Beta-Pinene	a29	Polygonum multiflorum	Fetidine	a139
Ligusticum wallichii	Borneol	a30	Polygonum multiflorum	N-Trans-Feruloyltyramine	a140
Ligusticum wallichii	Butylidenecyclohexane	a31	Polygonum multiflorum	Physcion	a141
Ligusticum wallichii	Caffeic Acid Dimethyl Ether	a32	Polygonum multiflorum	Polygalacic Acid	a142
Ligusticum wallichii	Camphene	a33	Polygonum multiflorum	Polygodial	a143
Ligusticum wallichii	Camphor	a34	Polygonum multiflorum	Questin	a144
Ligusticum wallichii	Choline	a35	Polygonum multiflorum	Resveratrol	a145
Ligusticum wallichii	Chrysanthemaxanthin	a36	Polygonum multiflorum	Rhein	a146
Ligusticum wallichii	chuanxiongzine	a37	Polygonum multiflorum	Tetrahydroxytaxadiene	a147
Ligusticum wallichii	Cibarian	a38	Carthamus tinctorius	1-Heptadecene	a148
Ligusticum wallichii	Citronellol	a39	Carthamus tinctorius	1-Hexadecene	a149
Ligusticum wallichii	Citronellyl Acetate	a40	Carthamus tinctorius	2-Hexanol	a150
Ligusticum wallichii	Cnidilide	a41	Carthamus tinctorius	3-Hexanol	a151
Ligusticum wallichii	Cnidium Lactone	a42	Carthamus tinctorius	Alpha-Onocerin	a152
Ligusticum wallichii	Cocaine	a43	Carthamus tinctorius	Arachidic Acid	a153
Ligusticum wallichii	Dibutyl Phthalate	a44	Carthamus tinctorius	Carthamidin	a154
Ligusticum wallichii	Enanthaldehyde	a45	Carthamus tinctorius	Carvacrol	a155
Ligusticum wallichii	Ethyl Hexadecanoate	a46	Carthamus tinctorius	Clerosterol	a156
Ligusticum wallichii	Ethyl Linoleate	a47	Carthamus tinctorius	Dehydroshikimic Acid	a157
Ligusticum wallichii	Ethyl Palmitate	a48	Carthamus tinctorius	Kaempferol	a158

Ligusticum wallichii	Ethylisoheptadecanoate	a49	Carthamus tinctorius	Lauric Aldehyde	a159
Ligusticum wallichii	Ethylisooctadecanoate	a50	Carthamus tinctorius	Linoleyl Acetate	a160
Ligusticum wallichii	Fenchone	a51	Carthamus tinctorius	Neocarthamin	a161
Ligusticum wallichii	Gamma-Terpinene	a52	Carthamus tinctorius	Neocembrene	a162
Ligusticum wallichii	Heptadecanol	a53	Carthamus tinctorius	Quercetin	a163
Ligusticum wallichii	Hexadecanoic Acid	a54	Carthamus tinctorius	Safranal	a164
Ligusticum wallichii	Hexadecanol	a55	Carthamus tinctorius	Sagittariol	a165
Ligusticum wallichii	Humulene	a56	Carthamus tinctorius	Stearin	a166
Ligusticum wallichii	Limonene	a57	Cyperus rotundus	Alpha-Cyperone	a167
Ligusticum wallichii	Linalool	a58	Cyperus rotundus	Beta-Selinene	a168
Ligusticum wallichii	Linoleic Acid	a59	Cyperus rotundus	Copadiene	a169
Ligusticum wallichii	L-Valine-L-Valine Anhydride	a60	Cyperus rotundus	Cyperene	a170
Ligusticum wallichii	Menthyl Acetate	a61	Cyperus rotundus	Cyperol	a171
Ligusticum wallichii	Methyl Eugenol	a62	Cyperus rotundus	Cyperolone	a172
Ligusticum wallichii	Methyl Hexadecanoate	a63	Cyperus rotundus	Isocyperol	a173
Ligusticum wallichii	Methyl Linoleate	a64	Cyperus rotundus	Isokobusone	a174
Ligusticum wallichii	Methyl Palmitate	a65	Cyperus rotundus	Kobusone	a175
Ligusticum wallichii	Methyl Pentadecanoate	a66	Cyperus rotundus	Patchoulene	a176
Ligusticum wallichii	Methyl Phenyl Carbinol	a67	Cyperus rotundus	Rotundone	a177
Ligusticum wallichii	Methyl Phenylacetate	a68	Cyperus rotundus	Sugetriol	a178
Ligusticum wallichii	Myrcene	a69	Rhizoma corydalis	(+)-Corydaline	a179
Ligusticum wallichii	Naphthalene	a70	Rhizoma corydalis	Allocryptopine	a180
Ligusticum wallichii	N-Butyl-2-Ethylbutylphthalate	a71	Rhizoma corydalis	Canadine	a181
Ligusticum wallichii	Neocnidilide	a72	Rhizoma corydalis	Canaline	a182
Ligusticum wallichii	O-Cresol	a73	Rhizoma corydalis	Columbamine	a183
Ligusticum wallichii	Octanol	a74	Rhizoma corydalis	Corchoroside A	a184
Ligusticum wallichii	O-Ethylphenol	a75	Rhizoma corydalis	Corycavine	a185
Ligusticum wallichii	Oleic Acid	a76	Rhizoma corydalis	Corydaline	a186
Ligusticum wallichii	P-Cymene	a77	Rhizoma corydalis	Corydalmine	a187
Ligusticum wallichii	Pentadecanoic Acid	a78	Rhizoma corydalis	Corydamine	a188
Ligusticum wallichii	Pentadecanol	a79	Rhizoma corydalis	Corydine	a189
Ligusticum wallichii	Pentylbenzene	a80	Rhizoma corydalis	Corytuberine	a190
Ligusticum wallichii	Perlolryne	a81	Rhizoma corydalis	Dehydrocorydaline	a191
Ligusticum wallichii	Retinol	a82	Rhizoma corydalis	Dehydrocorydalmine	a192
Ligusticum wallichii	Sabinene	a83	Rhizoma corydalis	Dehydrocostus Lactone	a193
Ligusticum wallichii	Senkyunolide B	a84	Rhizoma corydalis	Glaucine	a194
Ligusticum wallichii	Senkyunolide G	a85	Rhizoma corydalis	Isocorydine	a195
Ligusticum wallichii	Senkyunolide K	a86	Rhizoma corydalis	Isocorynoline	a196
Ligusticum wallichii	Spathulenol	a87	Rhizoma corydalis	Isocorypalmine	a197
Ligusticum wallichii	Terpinen-4-Ol	a88	Rhizoma corydalis	Isocrotonylpterosin B	a198
Ligusticum wallichii	Tetradecane	a89	Rhizoma corydalis	Methyl Leptol B	a199
Ligusticum wallichii	Tetramethylpyrazine	a90	Rhizoma corydalis	Norisocorydine	a200
Ligusticum wallichii	Thymol	a91	Rhizoma corydalis	Norjuzunal	a201
Ligusticum wallichii	Trans-Beta-Farnesene	a92	Rhizoma corydalis	Palmatine	a202
Ligusticum wallichii	Trans-Caryophyllene	a93	Rhizoma corydalis	Palmidin A	a203
Ligusticum wallichii	Vallesiachotamine	a94	Rhizoma corydalis	Protopine	a204
Ligusticum wallichii	Vitamin B1	a95	Rhizoma corydalis	Protoporphyrin	a205
Salvia miltiorrhiza	1-Hydroxytaxinine A	a96	Rhizoma corydalis	Reticulin	a206
Salvia miltiorrhiza	6-Hydroxymethylumazin	a97	Rhizoma corydalis	Reticuline	a207
Salvia miltiorrhiza	Cryptoxanthin	a98	Rhizoma corydalis	Scoulerine	a208
Salvia miltiorrhiza	danshensu	a99	Rhizoma corydalis	Stylopine	a209
Salvia miltiorrhiza	danshenxinkun A	a100	Rhizoma corydalis	Stypandrol	a210
Salvia miltiorrhiza	Daphneolone	a101	Rhizoma corydalis	Tetrahydrocorysamine	a211
Salvia miltiorrhiza	Dauricine	a102	Rhizoma corydalis	Tetrahydropalmatine	a212
Salvia miltiorrhiza	Dehydromiltirone	a103	Rhizoma corydalis	Thaliporphine	a213
Salvia miltiorrhiza	Dehydrotremetone	a104	Rhizoma corydalis	Yuanhunine	a214

Salvia miltiorrhiza	Dihydroisotanshinone I	a105	Rhizoma corydalis	Yuehchukene	a215
Salvia miltiorrhiza	Salvia miltiorrhiza	a106	Multiple drugs	20-Hexadecanoylingenol	T1
Salvia miltiorrhiza	Salvia miltiorrhiza	a107	Multiple drugs	Caffeicacid	T2
Salvia miltiorrhiza	Salvia miltiorrhiza	a108	Multiple drugs	Caffeicacid	T3
Salvia miltiorrhiza	Isocryptotanshinone	a109	Multiple drugs	Gamma-Sitosterol	T4
Salvia miltiorrhiza	Isocucurbitacin D	a110	Multiple drugs	Gamma-Sitosterol	T5

Supplementary Table 2. Core compounds.

TCM	Compounds	Betweenness centrality	Degree
Salvia miltiorrhiza	Tanshinone IIA	0.043	48
Salvia miltiorrhiza	Neotanshinone C	0.043	48
Salvia miltiorrhiza	Neocryptotanshinone II	0.043	48
Salvia miltiorrhiza	Miltionone I	0.043	48
Cyperus rotundus	Patchoulenone	0.0672	41

Supplementary Table 3. Molecular docking results of compounds and target proteins.

Compounds	Binding energies (kcal/mol)			
	ALB	IL6	INS	TNF
Miltionone I	-9.25 ± 0.29	-8.41 ± 0.02	-8.41 ± 0.02	-11.68 ± 1.28
Neocryptotanshinone II	-10.43 ± 0.56	-10.50 ± 0.20	-10.43 ± 0.15	-14.09 ± 0.13
Neotanshinone C	-10.19 ± 0.86	-8.69 ± 0.08	-8.93 ± 0.41	-13.05 ± 0.32
Patchoulenone	-9.98 ± 0.16	-9.61 ± 0.03	-9.60 ± 0.10	-13.24 ± 0.38
Tanshinone IIA	-8.73 ± 0.20	-8.80 ± 0.01	-8.80 ± 0.02	-13.14 ± 0.06